Effector-Triggered Immune Response in *Arabidopsis thaliana* Is a Quantitative Trait

Michail Iakovidis,* Paulo J. P. L. Teixeira,* Moises Exposito-Alonso,† Matthew G. Cowper,* Theresa F. Law,‡ Qingli Liu,* Minh Chau Vu,* Troy Minh Dang,* Jason A. Corwin,* Detlef Weigel,† Jeffery L. Dangl,*,‡,§ and Sarah R. Grant*,§,1

*Department of Biology, ‡Howard Hughes Medical Institute, and §Curriculum in Genetics and Molecular Biology, University of North Carolina, Chapel Hill, North Carolina 27599, and †Department of Molecular Biology, Max Planck Institute for Developmental Biology, Tübingen, 72076, Germany

ABSTRACT We identified loci responsible for natural variation in *Arabidopsis thaliana* (*Arabidopsis*) responses to a bacterial pathogen virulence factor, HopAM1. HopAM1 is a type III effector protein secreted by the virulent *Pseudomonas syringae* strain *Pto* DC3000. Delivery of HopAM1 from disarmed *Pseudomonas* strains leads to local cell death, meristem chlorosis, or both, with varying intensities in different *Arabidopsis* accessions. These phenotypes are not associated with differences in bacterial growth restriction. We treated the two phenotypes as quantitative traits to identify host loci controlling responses to HopAM1. Genome-wide association (GWA) of 64 *Arabidopsis* accessions identified independent variants highly correlated with response to each phenotype. Quantitative trait locus (QTL) mapping in a recombinant inbred population between Bur-0 and Col-0 accessions revealed genetic linkage to regions distinct from the top GWA hits. Two major QTL associated with HopAM1-induced cell death were also associated with HopAM1-induced chlorosis. HopAM1-induced changes in *Arabidopsis* gene expression showed that rapid HopAM1-dependent cell death in Bur-0 is correlated with effector-triggered immune responses. Studies of the effect of mutations in known plant immune system genes showed, surprisingly, that both cell death and chlorosis phenotypes are enhanced by loss of *EDS1*, a regulatory hub in the plant immune-signaling network. Our results reveal complex genetic architecture for response to this particular type III virulence effector, in contrast to the typical monogenic control of cell death and disease resistance triggered by most type III effectors.

KEYWORDS *Arabidopsis thaliana*; *Pseudomonas syringae*; type III effectors; HopAM1; QTL; genetics of immunity

PLANT pathogens have evolved complex strategies to circumvent the host innate immune response and enhance virulence, including the use of effector proteins to disrupt host immune signaling (Macho and Zipfel 2015). Plant immunity functions through extra- and intracellular receptor systems. Cell surface pattern-recognition receptors respond to pathogen molecules such as flagellin by activation of a complex defense signaling cascade called microbe (pathogen)-triggered immunity (MTI). MTI leads to production of reactive oxygen, secretion of pathotoxins, and reinforcement of cell walls at the infection site, which collectively protect the plant from infection. Successful pathogens introduce into host cells effector proteins that interact with components of the MTI response to dampen it, allowing the pathogen to evade host immunity. In response, the plant immune system evolved an intracellular class of highly polymorphic immune receptors, termed **n**ucleotide binding **l**eucine-rich **r**epeat (NLR) proteins (Bonardi and Dangl 2012). There are two classes distinguished by their N-terminal domains: Toll/interleukin-1 receptor domain (TIR)-NLRs that require the function of the defense protein EDS1, and coiled-coil (CC)-NLRs that are generally independent of EDS1 (Feys *et al.* 2001; Wiermer *et al.* 2005). These proteins can associate with targets of pathogen effectors that are presumably components of the MTI response, or decoys thereof (Dangl and Jones 2001; van der Hoorn and Kamoun 2008; Dodds and Rathjen 2010; Kroj *et al.* 2016). When the targets are perturbed by a

doi: 10.1534/genetics.116.190678
Manuscript received April 19, 2016; accepted for publication July 5, 2016; published Early Online July 12, 2016.
Available freely online through the author-supported open access option.
Supplemental material is available online at www.genetics.org/lookup/suppl/doi:10.1534/genetics.116.190678/-/DC1.
[1]Corresponding author: 4258 Genome Sciences Bldg., Department of Biology, CB#3280, University of North Carolina at Chapel Hill, 250 Bell Tower Dr., Chapel Hill, NC 27599-3280. E-mail: sgrant@email.unc.edu

pathogen effector, an associated NLR can be activated, leading to an effector-triggered immune response (ETI). ETI is often thought of as an amplified MTI response (Tao *et al.* 2003; Jones and Dangl 2006), commonly resulting in rapid cellular desiccation and death at the site of attempted infection (Wright and Beattie 2004). This hypersensitive cell death response can isolate microbial pathogens and halt their proliferation. Because effectors are required to suppress MTI, but can trigger ETI, successful pathogens are under evolutionary pressure to continuously "re-sort" their effector collections to suppress MTI while avoiding NLR receptor activation. This evolutionary tug of war has led to bacterial pathogens with diverse collections of effectors that often function through unusual chemistries or via convergent evolution to mimic eukaryotic enzymatic functions (Fu *et al.* 2007; Zhang *et al.* 2007; Cheong *et al.* 2014).

MTI and ETI are accompanied by dramatic changes in host hormone signaling and altered expression of thousands of host genes (Zipfel *et al.* 2004, 2006; Howard *et al.* 2013; Lewis *et al.* 2015). Pathogen effector proteins interact with specific host targets that potentially influence only a sector or branch of this host immune output. Identification of host targets of pathogen effectors has been a useful method to define and study subsets of the immune system and to understand how they contribute to immunity (Deslandes and Rivas 2012; Macho and Zipfel 2015). Here, we investigated the genetics of natural variation in plant responses to toxic effects of the *Pseudomonas syringae* type III secretion-system effector HopAM1. *P. syringae* pv. *tomato* DC3000 (*Pto* DC3000), a Gram-negative bacterium virulent on tomato and on *Arabidopsis thaliana* (*Arabidopsis*), is an extensively studied model pathogen for plant-microbe interactions (Chang *et al.* 2005; Schechter *et al.* 2006; Cunnac *et al.* 2011; Xin and He 2013; Lewis *et al.* 2015). *Pto* DC3000 has at least 30 type III effector genes including two nucleotide sequence-identical copies of *hopAM1*, one in the genome (PSPTO_1022) and one in the plasmid (PSPTO_A0005) (Buell *et al.* 2003). The *hopAM1* gene is sporadically dispersed among phylogenetically diverse *P. syringae* isolates (Arnold *et al.* 2001; Baltrus *et al.* 2011) and other Gram-negative plant pathogen groups, such as *Ralstonia*, *Xanthomonas*, and *Pantoea* (Integrated Microbial Genomes and Microbiomes, http://img.jgi.doe.gov/) (Nordberg *et al.* 2014). HopAM1 was originally identified from *P. syingae* pv. *pisi* via its ability to trigger a presumably NLR-mediated ETI response on some pea cultivars (Cournoyer *et al.* 1995). Addition of *hopAM1* to the effector complement of the weakly pathogenic strain *P. syringae* pv. *maculicola* (*Pma* M6CdE) conferred a growth advantage on *Arabidopsis* (Goel *et al.* 2008). Furthermore, *hopAM1* was one of eight type III effector genes that collectively restored nearly full virulence when added back to a completely growth-defective derivative of *Pto* DC3000, *Pto* DC3000D28E, from which the 28 most strongly expressed type III effector genes had been removed by sequential deletion (Cunnac *et al.* 2011). Like many other type III effectors, HopAM1 has toxic effects when overexpressed from a transgene in plants (Goel *et al.* 2008) and even in yeast (Munkvold *et al.* 2008). This latter phenotype has hampered approaches to define the biochemical function of HopAM1.

HopAM1 induces two unusual responses on *Arabidopsis* which are both variable across *Arabidopsis* accessions. HopAM1 can induce meristem chlorosis on many accessions; noted as emergence of chlorotic leaves 5–10 days after onset of HopAM1 expression when expressed from a conditionally induced transgene in *Arabidopsis*, or following inoculation of plant leaves with disarmed *Pseudomonas* strains designed to deliver HopAM1 by type III secretion. The effect appears to be systemic since it was not possible to recover any of the inoculated bacterial strain from the chlorotic leaves that emerged following hand inoculation of more mature leaves (Goel *et al.* 2008). Disarmed *Pseudomonas* strains expressing *hopAM1* can also induce local cell death in leaves at the infiltration site, and the timing of onset is variable across inbred *Arabidopsis* accessions. We exploited this natural variation in *Arabidopsis* responses to HopAM1 to define host loci that control them. Using linkage analyses in both experimental crosses and the global population to describe the genetic architecture of the response to HopAM1, we identified multiple loci associated with differential response to HopAM1 for both cell death and meristem chlorosis.

Materials and Methods

A. thaliana germplasm, propagation, and growth conditions

Seeds were germinated on a mix of potting soil (13:6:3 of Metro-Mix 360, baked sand, and Perlite; 1.4 g of Peters 20-20-20 All Purpose Fertilizer; and 0.85 ml of Marathon per liter of soil mix); stratified for 5 days at 4°; transferred to growth chambers; and grown for 9 hr under light (5900 lx), 15 hr in dark at 21° (day) and 18° (night) at 45–50% relative humidity. For propagation, plants were transferred to a long day (15 hr light) greenhouse with similar conditions. Plants for HopAM1-induced meristem chlorosis were prepared differently as described below. Col-0 × Bur-0 recombinant inbred line (RIL) population was obtained from Christine Camilleri (Institut National de la Recherche Agronomique, France) (Simon *et al.* 2008). *A. thaliana* accessions, mutant, and transgenic CS_ and SALK_ lines were obtained from the *Arabidopsis* Biological Resource Center (ABRC) (Ohio State University, Columbus, OH). The *eds1-2* line is a null mutant introgressed from a mutant in the accession Ler-0 into the Col-0 background (Bartsch *et al.* 2006). Mutant lines *axr2-1*, *abi1-1*, and *aba2* were obtained from Jason Reed (University of North Carolina, Chapel Hill, NC) (Nagpal *et al.* 2000); *ein2-5* and *ein2-50* from Joseph Kieber (University of North Carolina, Chapel Hill, NC) (Wang *et al.* 2007); the *global* DELLA quintuple mutant from Salomé Prat (Centro Nacional de Biotecnologia, Madrid, Spain) (Cheng *et al.* 2004); and the triple TOC64 mutant from Úrsula Flores Pérez (Oxford University, Oxford, United Kingdom) (Aronsson *et al.* 2007).

Bacterial strains and growth assay

A list with strains and phenotypes assayed can be found in Supplemental Material, Table S1. Bacterial strains were maintained and grown as described (Chung *et al.* 2011) and *in planta* growth assays were done as described (Chang *et al.* 2005). Bacterial strains were grown in King's B liquid media at 28° with shaking overnight. Antibiotic concentrations used for *P. syringae*, *P. fluorescens*, and *P. maculicola* were: 50 μg/ml rifampicin, 50 μg/ml kanamycin, 10 μg/ml spectinomycin, and 5 μg/ml tetracyclin. Weighted ANOVA was used to compare bacterial growth differences between strains from multiple experiments in Col-0 and Bur-0. Comparisons among the groups were done using Tukey's *post hoc* test.

DNA extraction and PCR conditions for genotyping

We modified the protocol from Klimyuk *et al.* (1993) as follows. Plant material (one to two young leaves) was harvested and placed in a well (Deepwell plate 96/2000 μl; Eppendorf) along with a 4-mm borosilicate glass ball and 400 μl 0.25 M NaOH. Samples were then homogenized at 1200 strokes/min for 1 min (2000 GENO/GRINDER; Spex-CentriPrep). Plates were centrifuged for 1 min at 1000 rpm to precipitate plant tissue. A 50 μl volume of supernatant was transferred into a 96-well PCR plate (nonskirted; MultiMax) and heated at 96° for 30 sec in a Peltier thermal cycler (DNA Engine; Bio-Rad, Hercules, CA) with open lid. A 50 μl volume of 0.25 M HCl was added to neutralize the sample, and 25 μl of alkaline lysis buffer (0.5 M Tris-HCl, pH 8.0, 0.25% v/v IGEPAL CA-630) was added immediately after, mixing the samples by pipetting. The PCR plate was heated again at 96° for 120 sec and left to cool at room temperature for 5 min. A 1–2 μl volume of DNA sample was used for PCR for genotyping. PCRs were set for a 7 min "hot-start" step at 95°, followed by 35 cycles of 30 sec 95° denaturation, 30 sec *X* (primer-specific)° annealing, 60 sec 72° extension, and concluding with a 5 min 72° final extension. Optimized 10× PCR buffer [0.11 M KCl, 0.11 M $(NH_4)_2SO_4$, 0.24 M Tris-HCl (pH 8.3), 0.022 M $MgCl_2$, 0.6% v/v Triton X-100, 1.6% v/v Tween 20, 1.2% v/v NP-40, 1.5% v/v formamide, 0.1 mg/ml BSA, 10% v/v glycerol, and 0.02 M TMAC] was used for genotyping.

HopAM1-induced cell death assay

Cell death symptoms induced by bacteria were scored following trypan blue staining (Boyes *et al.* 1998) at various time intervals. Plants that were 5- to 6-weeks old were hand inoculated with bacteria. Inocula with *Pto*-derived strains were adjusted to an OD_{600} of 0.1 ($\sim 5 \times 10^7$), and with *Pfo* or *Pma* strains to an OD_{600} of 0.2 ($\sim 1 \times 10^8$ CFU/ml) in 10 mM $MgCl_2$. For phenotyping, 3–4 leaves of 5-week-old plants were marked with a Sharpie felt pen on the axial side and the abaxial side was hand inoculated with *Pto* DC3000D28E (*hopAM1*) (see Table S1), and scored for cell death response at 24, 26, 32, 48, 72, and 96 hpi (Figure 1C). Quantitative scoring of cell death symptoms ranged from 5 (apparent by 24 hpi) to 0 (not apparent by 96 hpi) based on the time point that symptoms were first observed.

HopAM1-induced meristem chlorosis assay

Tissue culture plates (six well, #353046; Falcon, Lincoln Park, NJ) were filled with sifted soil mix (prepared as described in Boyes *et al.* 1998; Holt *et al.* 2002). Each plate was then covered with nylon mesh and fastened with four wide rubber bands. Four plastic head pins were placed inside the corners of each plate to provide aeration during germination and support during vacuum infiltration. A total of 5–10 seeds were sown on each soil mount, plate lids were then placed on the pins, and plates were moved to 4° for 4–5 days. Seedlings were thinned to a single plant in the middle of each mount. Three 4-week-old plants per line were vacuum infiltrated with *Pto* DC3000D28E(*hopAM1*) and scored for chlorotic rosette phenotype at 10 days post inoculation (dpi): Plates were placed inverted in a rectangular plastic container filled with bacterial inoculum (OD_{600} of 0.05 ($\sim 2.5 \times 10^7$ CFU/ml), 10 μM $MgCl_2$, 60 μl/liter Silwet L-77 surfactant), 4-cm deep, and vacuum was applied for 100–120 sec. Plants were transferred into growth rooms. Phenotypic scores were assigned based on visible chlorosis in rosettes at 10 dpi. The phenotype was recorded as "any response" (1) or "no response" (0).

QTL analysis

Cell death: Three F_8 plants each of 342 lines from a Col-0 × Bur-0 RIL mapping population (Simon *et al.* 2008) were scored for HopAM1-induced cell death, following hand inoculation with *Pto* DC3000D28E(*hopAM1*). Initial QTL analysis on the 89 markers spanning five chromosomes of *A. thaliana* was performed by composite interval mapping (CIM) using WinQTL Cartographer 2.5.011 (Wang *et al.* 2012). After the detection of several QTL, the entire RIL population was reannotated using 60 additional markers to provide extra resolution for CIM. New markers were selected proximally and distally for each marker within the QTL regions detected. Mapping distances were recalculated using MapMaker 3.0 (Lincoln *et al.* 1992). For detecting QTL, a LOD score of 3.2 was chosen based on 1000 permutations at $P \leq 0.01$ for CIM. Walking speed was 0.5 cM and window size was 10 cM. Epistatic interactions between the QTL identified in CIM were investigated in detail using a general linear model structure (Brady *et al.* 2015), which provides more power than traditional pairwise *t*-tests in factorial interaction studies, by using the ANOVA framework.

Meristem chlorosis: Three plants per Col-0 × Bur-0 RIL (Simon *et al.* 2008) were scored for HopAM1-induced meristem chlorosis at 10 and 14 dpi, following vacuum infiltration with *Pto* DC3000D28E(*hopAM1*). CIM was performed again on the original genotyping data (89 markers) and the reannotated data (89 + 60 markers). QTL was detected as in *Cell death* above. Other parameters were set at default. The model for corrected means that was used before for

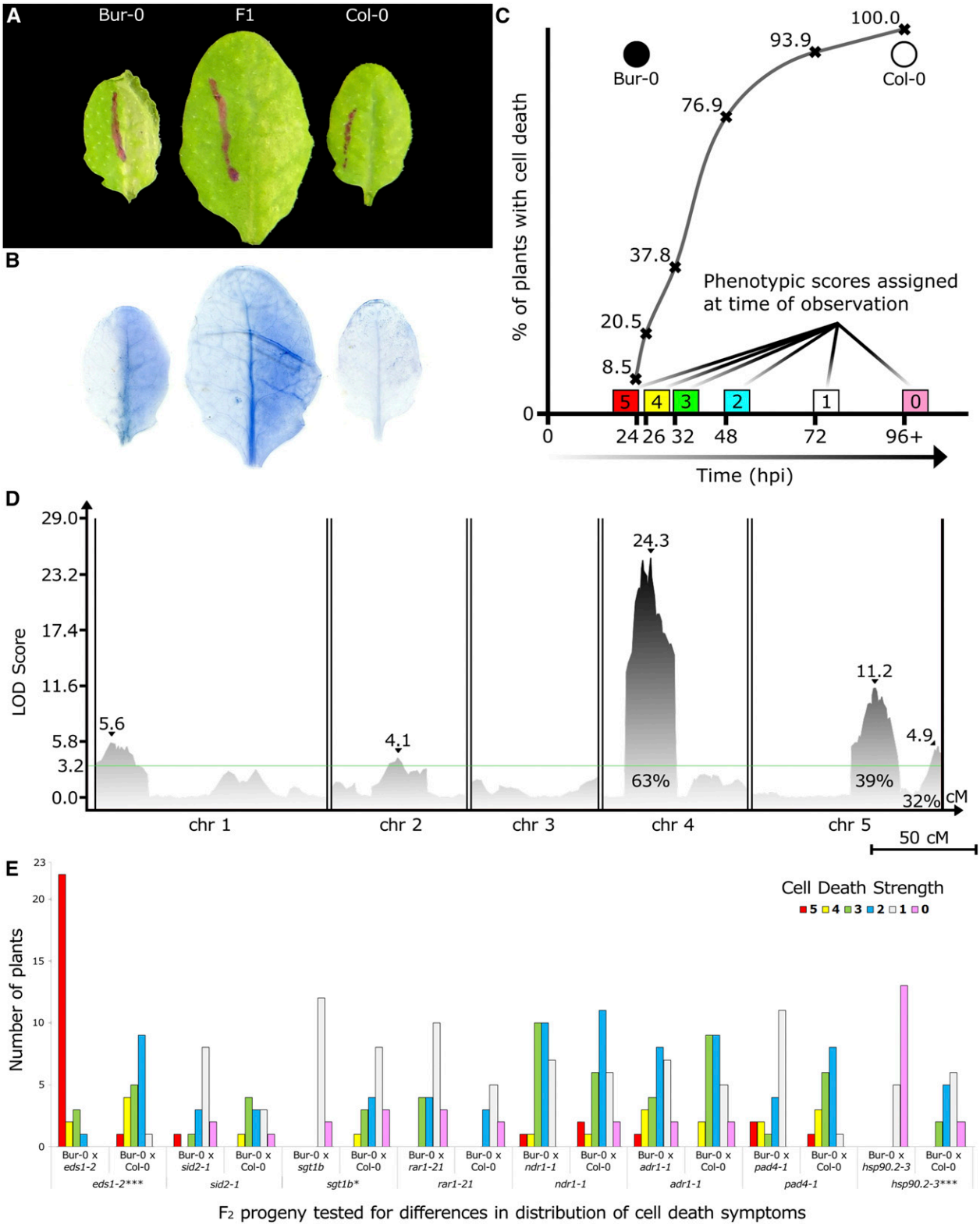

Figure 1 HopAM1 induces variable cell death symptoms of multigenic inheritance in *A. thaliana* accessions. (A) HopAM1-induced cell death in Bur-0, Col-0, and F_1 progeny at 48 hpi after hand inoculation with *Pto* DC3000D28E(*hopAM1*). OD_{600} = 0.1 (~5 × 10^7 CFU/ml). Bur-0 exhibits one of the strongest onsets of symptoms as early as 23 hpi, while Col-0 exhibits only chlorosis starting ~96 hpi. F_1 progeny become symptomatic ~48 hpi. (B) Cell death shown with trypan blue staining on the same leaves as above (48 hpi). (C) Sigmoid distribution of cell death symptoms representative of quantitative traits. The quantification of cell death at specific time points postinoculation is shown. Curve shows the percentage of plants in a Bur-0 × Col-0 RIL population that exhibit cell death symptoms at a given time point. ● = Bur-0; ○ = Col-0. (D) CIM on 342 reannotated RILs from a Col-0 × Bur-0 collection. The *x*-axis displays chromosomes 1 through 5 with map distances in cM. Peak LOD scores are shown by ▼ along with their values.

HopAM1-induced cell death (see Table S2) was not suitable for the binary nature of phenotypes for HopAM1-induced meristem chlorosis and was not included in the model. Phenotypic scores for all 342 RILs were assigned as observed (with at least one responsive replicate resulting in a score of 1). Symptoms similar to HopAM1-induced cell death and meristem chlorosis have not been observed before in untreated Col-0 × Bur-0 RILs (Simon *et al.* 2008; Gery *et al.* 2011; Chavigneau *et al.* 2012).

Genome-wide association (GWA) analysis: To obtain a species-wide view of HopAM1-induced cell death and meristem chlorosis, we assayed 98 *A. thaliana* accessions (ABRC). For most of our accessions (n = 64), whole-genome sequences were available (http://1001genomes.org; 1001 Genomes Consortium 2016). We used 4,004,754 SNPs with 0.98 genotyping rate and minor allele frequency (MAF) >5% to perform GWA analyses, using a linear mixed model to correct for population structure, implemented in the Efficient Mixed-Model Association eXpedited (EMMAX) package (Kang *et al.* 2010), as this has been proven to be efficient for *Arabidopsis* (Atwell *et al.* 2010). This model fits an additive genetic variance factor using a kinship matrix, which allows calculation of narrow sense heritability for the GWA population. To test the significance of the genetic variance factor, we used a likelihood ratio test comparing the fit of the full model against the null model without the kinship matrix. Allele effect sizes were reported as standardized regression coefficients or β. They are interpreted as the difference between genotypes carrying the MAF allele to those with the reference allele, and are expressed in standard deviations of the phenotype. Enrichment of top SNPs in QTL peaks was tested using a Fisher's exact test with two-by-two tables of counts as follows:

Top GWA SNPs inside QTL range: total SNPs inside QTL range.

Top GWA SNPS in the chromosome of the QTL: total SNPs in the chromosome of the QTL.

Confocal microscopy: Small leaves (5-mm diameter) were collected 14 days after vacuum infiltration with *Pto* DC3000(*hopAM1*). The abaxial side of Col-0 and Bur-0 leaves was observed using a C-Apochromat 40×/NA1.2 water immersion lens on a Carl Zeiss (Thornwood, NY) LSM710 confocal laser scanning microscope. Autofluorescence was observed using a 560-nm diode laser line for excitation and the photomultiplier tube detector collected emission bandwidth set at 568–740 nm. The confocal images were edited with ZEN 2009 software.

RNA sequencing: We used RNA sequencing (RNA-seq) to investigate HopAM1-associated changes in the transcriptome of infected *Arabidopsis* leaves. Plants that were 5 weeks old and grown under short days were hand-infiltrated (OD_{600} = 0.1, ~2.5 × 10^7 CFU/ml) with the control strain *Pto* DC3000D28E transformed with the empty vector pJC531; or with *Pto* DC3000D28E(*hopAM1*) (Goel *et al.* 2008). The accessions Col-0 and Bur-0 were used in the experiment. Samples were harvested immediately before (time = 0 hr) and 2, 4, 6, 8, 10, and 12 hr after bacteria infiltration. Three biological replicates were analyzed per condition, each consisting of three 7-mm disks collected from the inoculated leaf of one individual plant. Samples were frozen in liquid nitrogen and ground using glass beads and the Tissue Lyser II system (QIAGEN, Valencia, CA). Total RNA was extracted using TRIzol (Invitrogen, Purchase, NY), DNase (Ambion Turbo DNase) treated, and purified using the RNeasy Mini Kit (QIAGEN). A 1 μg amount was used to prepare Illumina-based mRNA-seq libraries. Quality control and quantification of the final libraries were performed using the 2100 Bioanalyzer (Agilent) and the Quant-iT PicoGreen dsDNA Reagent (Invitrogen). Barcoded libraries were combined into a single pool and sequenced in two lanes of an Illumina HiSeq2500, resulting in an average of 2.1 million 50-bp single-end reads per library.

RNA-seq reads were mapped using TopHat (Trapnell *et al.* 2009), allowing only one mismatch and discarding any read that mapped to multiple positions. The TAIR10 assembly was used as the reference genome for Col-0, whereas the assembly available at http://mus.well.ox.ac.uk/19genomes/ was used as the reference for Bur-0 (Schneeberger *et al.* 2011). Approximately 90% of reads could be mapped to the *Arabidopsis* genome. Reads mapped to nuclear protein-coding genes were counted using HTSeq (Anders *et al.* 2015) and the package edgeR (Robinson *et al.* 2010) was used to define differentially expressed genes between plants infiltrated with *Pto* DC3000D28E(*hopAM1*) and *Pto* DC3000D28E(EV) at each time point. Genes with a false discovery rate (FDR) <0.05 and a fold-change variation >2 were considered differentially expressed between conditions. All nuclear protein-coding genes were tested for differential expression without the adoption of thresholds to filter out weakly expressed genes. Gene ontology (GO) enrichment analyses were performed with the PlantGSEA platform (Yi *et al.* 2013) using the sets of differentially expressed genes. Transcriptional activation of chosen gene sets was represented as the median z-score transformed expression values [in **r**eads **p**er **k**ilobase of transcript per **m**illion (RPKM) mapped reads].

Effects on phenotype variation are shown as percentages for QTL4 and QTL5A. The global permutation level of significance was set on LOD 3.2. Chr, chromosome. Bar, 50 cM. (E) Distribution of HopAM1-induced cell death scores among different F_2 progeny between Bur-0 and mutant lines. The *y*-axis shows number of plants selected from each population with each phenotype score for HopAM1-induced cell death (5 = Bur-0, 0 = Col-0). Statistical significance between distributions was based on two-way ANOVA tests for each pair (statistical significance: *** $P \leq 0.001$, * $P \leq 0.05$).

Data availability

Bacterial strains are available upon request. All data necessary for reproducing QTL results and complete edgeR results for RNA-seq data can be found as supplemental materials. Raw RNA-seq data are available at the National Center for Biotechnology Information Sequence Read Archive under the accession number SRP075162.

Results

The quantitative nature of HopAM1-induced cell death

Previously, we cloned 93 type III secretion system effectors from *P. syringa*e isolates (Baltrus *et al.* 2011) and transferred them individually into an engineered strain of the nonpathogenic *P. fluorescens* bacterium carrying a heterologous type III secretion system apparatus (Thomas *et al.* 2009). Disease resistance responses are often qualitative, and we hoped to identify several such host responses across this survey. HopAM1 induced obvious cell death in some accessions. To better define the distribution of phenotypes across the host species and to identify accessions that would be suitable for mapping in experimental crosses, we rescreened a collection of 98 accessions delivering HopAM1 by infection with the disarmed bacterial strain *Pto* DC3000D28E (Cunnac *et al.* 2011) bearing a plasmid with the *hopAM1* gene with a C-terminal HA tag expressed from its own promoter (Goel *et al.* 2008). Although its virulence is severely reduced, *Pto* DC3000D28E stimulates MTI effectively and is at least as effective as *P. fluorescens* for delivery of type III effectors. Following hand inoculation of leaves with *Pto* DC3000D28E(*hopAM1*), we observed a range of cell death responses at the site of inoculations that varied between *Arabidopsis* accessions in the timing of onset of cell collapse (see Figure S1 and Table S3). Bur-0 showed strong cell death symptoms at 24 hpi; and Col-0 did not suffer from any symptoms, not even microscopic lesions visible with trypan blue staining (see Figure S2), until 6 dpi (~144 hpi) (Figure 1, A and B). Analysis of an F_2 population (468 plants) of Bur-0 × Col-0 demonstrated non-Mendelian segregation of HopAM1-induced cell death (see Table S4). Therefore, we followed the timing of appearance of cell death symptoms after inoculation to derive a quantitative cell death score (Figure 1C).

Screening and reannotation of Bur-0 × Col-0 RILs

We explored the genetic architecture driving HopAM1-induced cell death using an established Bur-0 × Col-0 F_8 RIL population (Simon *et al.* 2008) screened with *Pto* DC3000D28E (*hopAM1*). Cell death symptoms developed continuously over time after inoculation (see Figure S2) in the RIL population and phenotyping was performed following the numerical scoring system illustrated in Figure 1C. Two individual plants from each RIL were infiltrated with *Pto* DC3000D28E(*hopAM1*) and tissue was harvested from both for genotyping (see Table S5). The distribution of phenotypic scores among the RILs was similar (see Figure S3) to the distribution of the 98 *A. thaliana* accessions screened previously, where most lines presented with intermediate cell death phenotypes (Kolmogorov–Smirnov test for similarity between distributions; $D = 0.18$, $P = 0.014$) (see Figure S1). The parental accessions Col-0 and Bur-0 had the most extreme phenotypes, and there was no transgressive segregation among RILs. To evaluate the heritability of the cell death response in the RILs, a second screen of the RIL population was performed, and the initial phenotypic scores were adjusted to control for environmental effects using a general linear model (see Table S2) (Chan *et al.* 2011; Brady *et al.* 2015). The broad sense heritability (H^2) within the RILs for HopAM1-induced cell death was high ($H^2 = 95.4\%$, $P < 2 \times 10^{-16}$), with a very low amount of phenotypic variation being controlled by combined experimental factors ($H^2 = 0.06\%$) (see Table S2).

Five Arabidopsis loci additively control HopAM1-dependent cell death in the Bur-0 × Col-0 cross

CIM performed among the RILs identified five loci on chromosomes 1 (QTL1 = 0.0–8.4 Mb), 2 (QTL2 = 8.7–11.1 Mb), 4 (QTL4 = 0.0 – 5.79 Mb), and 5 (QTL5A = 16.3–21.3 Mb; QTL5B = 25.9–26.9 Mb) (Figure 1D; Table S6) (Wang *et al.* 2012). We screened putative heterogeneous inbred families (HIFs) derived from the RIL population for segregation at QTL4, QTL5A, and QTL5B to fine map the loci controlling HopAM1-induced cell death in the Bur-0 × Col-0 background. We progeny tested several RILs with a heterozygous haplotype for the QTL region of interest to identify segregating lines and then chose a few lines for subsequent fine mapping of each QTL (see Figure S4). QTL4 was delimited within the centromeric region of chromosome 4 (in Col-0 containing many genes of unknown function, several cysteine-rich receptor-like kinases, and one TIR-NLR, At4g04110). However, due to low recombination near the centromere, we could not reduce the size of the associated interval further. Thus, we focused our fine-mapping efforts on QTL5A and QTL5B. QTL5A was delimited within 296 kb (18.682–18.978 Mb) [containing genes of various function, including many TIR-NLR genes and the plasma-membrane localized receptor kinase protein FLS2 (At5g46330), which recognizes bacterial flagellin peptides that stimulate MTI responses (Zipfel *et al.* 2004)]. QTL5B was delimited to within 110 kb (26.639–26.749 Mb) (containing 30 genes, including MAPKK kinases and CC-NLR genes). The Col-0 gene annotations for the regions in QTL4, 5A and 5B, are listed in Table S7. We found only additive effects between the QTL using an ANOVA for each QTL pair from the initial CIM mapping to identify pairwise epistasis contributing to the HopAM1-induced cell death response (see Figure S5; Table S8) (Brady *et al.* 2015). However, our population sizes may be too small to effectively evaluate higher order epistasis (Joseph *et al.* 2013; Taylor and Ehrenreich 2014).

HopAM1-induced cell death is affected by EDS1, HSP90.2, and SGT1B

To assess if HopAM1-induced cell death is affected by genes known to be required for disease resistance, we made several

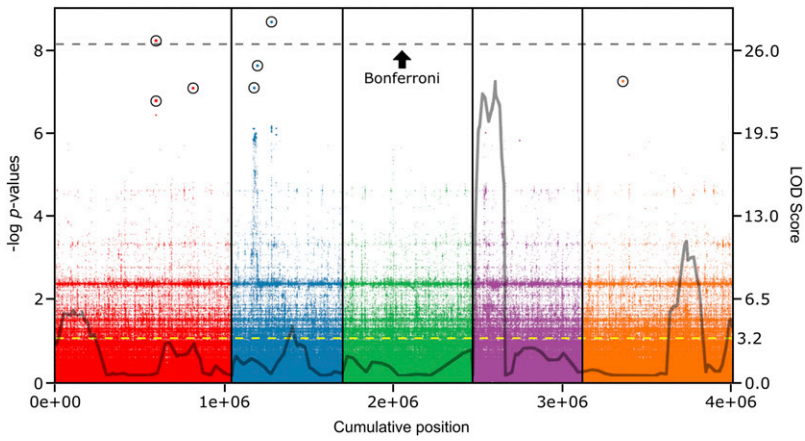

Figure 2 The genetic architecture of HopAM1 cell death response defined by GWA depends on several loci with strong to moderate effects. HopAM1-induced cell death response was scored in a collection of 64 *Arabidopsis* accessions. EMMAX was used for GWA mapping based on whole-genome sequence data of >4 million SNPs. The Manhattan plot shows the association of each SNP and its *P*-value across the five *Arabidopsis* chromosomes (1 through 5 from left to right, separated by vertical lines). The dotted line designates the significance threshold for Bonferroni correction ($P \leq 1.2 \times 10^{-8}$). All SNPs over the FDR threshold are highlighted with a circle. Gray outline reprises the QTL regions identified in Figure 1D in the Bur-0 × Col-0 background (cM converted to Mb only for each genetic marker's coordinates on the genome and shows LOD score at that specific location; not identical, but very similar to peak LOD scores shown in previous QTL analysis in Figure 1D). Right *y*-axis, LOD score; yellow dotted line, significance threshold for CIM.

crosses between the Bur-0 accession and Col-0 loss-of-function mutants in defense-related genes: *sid2-1* (Wildermuth *et al.* 2001), *sgt1b* (Austin *et al.* 2002), *rar1-21* (Tornero *et al.* 2002), *ndr1-1* (Century *et al.* 1995), *eds1-2* (Bartsch *et al.* 2006), *hsp90.2-3* (Hubert *et al.* 2003), *pad4-1* (Glazebrook *et al.* 1996), and *adr1-1* (Grant *et al.* 2003). A total of 96 F_2 progeny from each cross were genotyped and plants homozygous at markers flanking each Col-0-derived mutation in the respective crosses were selected for cell death phenotyping. As a comparative control, 96 plants from a Bur-0 × Col-0 F_2 progeny were screened for cell death and subsequently genotyped with the same markers used for the specific mutation in each cross. In Figure 1E, the phenotypes of the F_2 plants homozygous for a Col-0-derived mutant allele from the Col-0 mutant × Bur-0 cross are presented next to the phenotypes of plants from the subset of control Bur-0 × Col-0 F_2s which were homozygous for the wild-type Col-0 allele for the relevant gene. Our results indicated that *eds1-2*, *hsp90.2-3*, and *sgt1b* affect HopAM1-induced cell death symptoms from Bur-0 (Figure 1E). Homozygosity for either the *hsp90.2* ($hsp90.2_{Col\text{-}0}$) or *sgt1b* mutant allele ($sgt1b_{Col\text{-}0}$) in Bur-0 × Col-0 background attenuated HopAM1-induced cell death symptoms compared to their respective Bur-0 × Col-0 control populations. Because HSP90.2 and SGT1b are part of a steady-state NLR chaperone complex required for NLR ETI receptor activation (Hubert *et al.* 2003; Holt *et al.* 2005; Shirasu 2009), this is consistent with the hypothesis that at least one of the cell death QTL loci (Figure 1D) contains a functionally relevant NLR gene. The *eds1-2* mutation in the Bur-0 × Col-0 background enhanced the onset of HopAM1-induced cell death symptoms (Figure 1E), which was unexpected because EDS1 is required for the function of TIR-NLR proteins (Feys *et al.* 2001). The other defense mutations we tested had no effect.

GWA reveals additional loci associated with HopAM1 cell death

A disadvantage of QTL experiments is that the identified loci may represent rare, deleterious alleles compared to the entire population surveyed. GWA screens can complement QTL studies by identification of loci that do not have segregating alleles in the two RIL founder populations (Gibson 2012; Weigel and Nordborg 2015). We used 64 of the 98 accessions we had screened previously for a GWA study (see Table S3) because whole-genome resequencing data were available for them (http://1001genomes.org; 1001 Genomes Consortium 2016). The most significantly associated SNPs did not overlap with the intervals defined by the Bur-0 × Col-0 QTL analysis (Figure 2) but we found enrichment in the QTL regions when we considered the 50 (or more) most significantly associated SNPs in the same chromosome as the QTL (Table 1). The narrow sense heritability calculated for this study was $h^2 = 34.5\%$ (likelihood-ratio test, $P = 0.430$) and the allele frequencies of the SNPs with the strongest allele effects were generally shifted toward low MAF (see Figure S6A), consistent with a polygenic architecture for the trait according to an infinitesimal model (Gibson 2012). The SNPs most significantly associated with variation in HopAM1-induced local cell death were two peaks with multiple significantly associated SNPs on chromosome 2, and single SNPs on chromosomes 1 and 2 (Figure 2). A total of 5 out of the 10 most significant SNPs fell within a 154-bp noncoding region between At1g50420, encoding the scarecrow-like 3 (SCL3) transcription factor, a positive regulator of gibberellic acid signaling (Zhang *et al.* 2011) and At1g50430 (*STEROL Δ-7 REDUCTASE*), which encodes a sterol reductase involved in brassinosteroid synthesis (see Table S9) (Lecain *et al.* 1996). The most significantly associated SNP was on chromosome 2 in the fourth exon of *CYCLOPHILIN40* (At2g15790), which encodes a protein isomerase that functions in maturation of the AGO1-containing RNA-induced silencing complex important to epigenetic gene regulation (Romano *et al.* 2004; Smith *et al.* 2009; Iki *et al.* 2012). Aligning the haplotypes available from the 1001 Genomes Project that were used in our GWA over a 30-kb region spanning the *CYCLOPHILIN40* gene showed a correlation between haplotype and the HopAM1-dependent cell death phenotype (see Figure S7 and File S1).

Table 1 P-values of enrichment tests of increasing numbers of most significant SNPs for each HopAM1-induced cell death QTL

Number of top SNPS	10	50	100	500	1000	10000
QTL1	0.489	0.995	0.579	0.643	0.909	1
QTL2	0.818	1	1	1	1	1
QTL4	0.0906	0.0278	3.10×10^{-13}	2.88×10^{-46}	2.14×10^{-66}	1.52×10^{-08}
QTL5A	0.537	0.0434	1.55×10^{-06}	0.00942	0.0088	3.73×10^{-07}
QTL5B	1	1	1	7.04×10^{-06}	0.00021	0.00021

Calculated using a Fisher's exact test with a two-by-two test table design.

Other biparental populations have HopAM1-induced cell death QTL that overlap with Bur-0 × Col-0 QTL5A

To explore the differential genetic architecture driving HopAM1-induced cell death among the accessions, we screened three different biparental mapping populations to investigate whether HopAM1-induced cell death is also a quantitative trait in other accessions. We scored plants from three other populations with parents divergent in their cell death phenotypes, but not as divergent as Bur-0 × Col-0: a Ler-0 × Col-4 RIL population (CS1899), a Sha × Col-0 F_2 population, and a Ws-2 × Col-0 F_2 population for HopAM1-induced cell death (see Table S10). Ler-0 and Ws-2 had cell death scores of 2 and the Sha score was 4 (see Table S3). All three populations exhibited a continuous phenotypic response similar to the Bur-0 × Col-0 background, but with weaker phenotypes. We again observed no transgressive segregation. We performed a CIM analysis to identify the loci controlling the trait in all three backgrounds and to search for overlap with the loci identified in the Bur-0 × Col-0 background (see Figure S8). In the Ler-0 × Col-4 background, two QTL were identified on chromosome 1 (16.1–22.2 Mb) and chromosome 5 (15.4–20.9 Mb), and in the Ws-2 × Col-0 and Sha × Col-0 backgrounds, one QTL was identified that was solely responsible for the HopAM1-induced cell death (chromosome 5; 14.7–23.8 Mb for Ws-2 × Col-0, and 8.4–20.1 Mb for Sha × Col-0). The QTL identified on chromosome 5 for all three mapping populations (Ler-0 × Col-4, Ws-2 × Col-0, and Sha × Col-0) overlapped with QTL5A from the Bur-0 × Col-0 RIL population (16.3–21.3 Mb), possibly suggesting that the common parent, Col-0/Col-4, carries an unusual allele at this locus.

HopAM1-induced cell death and chlorosis are not associated with bacterial growth restriction in both Col-0 and Bur-0

HopAM1 induces obvious phenotypes, but it is unclear how these might be related to the restriction of pathogen growth, the effect most relevant to the host. HopAM1 enhances the growth of a weakly virulent *P. syringae* strain *Pma* (M6CdE) in the Ws-2 accession, but not in several other accessions tested (Goel *et al.* 2008). Thus, HopAM1 is a weak virulence factor, at least on Ws-2. To determine if the different cell death responses of Bur-0 and Col-0 to HopAM1 were correlated with differences in the ability to restrict pathogen growth via recognition of HopAM1, we infected Bur-0 and Col-0 with *Pto* DC3000. This strain grew to levels associated with disease in both accessions (Figure 3), with slightly higher titers in Bur-0. To determine if the endogenous *hopAM1* genes affect the growth of *Pto* DC3000 in these accessions, we infected Col-0 and Bur-0 with a *Pto* DC3000 derivative, *Pto* JB206, which lacks both the chromosomal (PSPTO_1022) (Boch *et al.* 2002) and plasmid-borne (PSPTO_A0005) (Landgraf *et al.* 2006) copies of *hopAM1*. We found a small, statistically significant, growth advantage of *Pto* JB206 over *Pto* DC3000 in both Bur-0 and Col-0 (Figure 3). This growth advantage disappeared from both accessions when *Pto* JB206 was complemented with the plasmid carrying *hopAM1* (Figure 3). Thus, HopAM1 is recognized by both accessions, at least to an extent sufficient to trigger growth restriction and there is no genetic difference between Bur-0 and Col-0 for this pathogen growth restriction. We infer that both accessions recognize and respond to HopAM1 at levels sufficient to trigger weak ETI; however only in Bur-0 does the signal delivered by HopAM1 result in ETI-associated cell death.

Overlapping and distinct QTL for HopAM1-induced meristem chlorosis and cell death

HopAM1 induces a chlorotic phenotype in newly developed leaves when delivered by a bacterial strain (*Pma* M6CdE) via hand infiltration or following transgenic expression of *hopAM1* in *Arabidopsis* (Goel *et al.* 2008). An improved vacuum infiltration assay was devised using *Pto* DC3000D28E (*hopAM1*) (see *Materials and Methods*). All 64 accessions used in our GWA for HopAM1-induced cell death response (see Table S3) were rescreened for HopAM1-induced meristem chlorosis. While most of the accessions exhibited meristem chlorosis at 7 dpi, 12 remained nonchlorotic (see Table S11). In fact, Col-0 exhibited strong meristem chlorosis and Bur-0 was nonresponsive, highlighting the contrasting underlying genetics of these two accessions in response to HopAM1 (Figure 4A). Of the three accessions that exhibited the highest cell death scores (Bur-0, Hov-4, and Wil-2; see Table S11), only Bur-0 did not exhibit HopAM1-induced meristem chlorosis. Hence, HopAM1 cell death and meristem chlorosis-inducing activities are not mutually exclusive. Confocal laser microscopy of Col-0 and Bur-0 newly emerged chlorotic leaves at 14 days after infection revealed that the chloroplasts in Col-0 were smaller, deformed, and exhibited a much weaker fluorescence signal; while the chloroplasts in the corresponding leaves in Bur-0 appeared normal (Figure 4B). Furthermore, Col-0 chlorotic leaf tissue had smaller, round-shaped mesophyll cells, while Bur-0 had wild-type cell

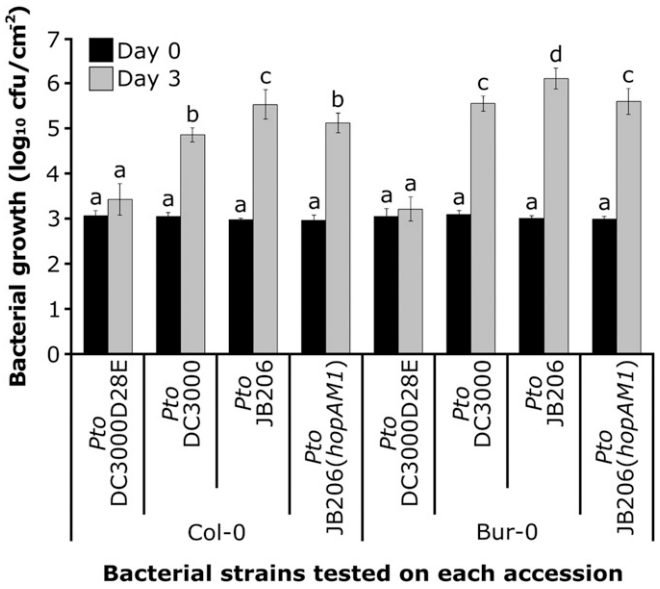

Figure 3 HopAM1 causes reduced growth of *P. syringae* in Col-0 and Bur-0 accessions, independent of cell death symptoms. Bacterial growth in Col-0 and Bur-0 accessions. The experiment is representative of five independent replicates; two times the SE between the means is noted by error bars. A weighted ANOVA test was applied to the difference in growth of the strains carrying *hopAM1* (*Pto* DC3000 and *Pto* JB206 +AM1) compared with the growth of the *hopAM1* deleted strain (*Pto* JB206). Statistical significance is indicated by letters based on the weighted ANOVA test ($P < 0.1$).

morphology (Figure 4B). We used the Bur-0 × Col-0 RIL population (Simon *et al.* 2008) again to identify loci controlling the HopAM1-induced meristem chlorosis. To assess the heritability of the meristem chlorosis trait in the RILs, we performed a second screen of a subset of the RIL population (162 lines with the highest number of recombination events were chosen). We tested the influence of environmental effects on our meristem chlorosis phenotype scores using a general linear model as before (see Table S12) (Chan *et al.* 2011). The broad sense heritability of the HopAM1-induced meristem chlorosis trait was $H^2 = 60.7\%$ ($P < 2 \times 10^{-16}$). Using the reannotated Bur-0 × Col-0 RILs, we performed a CIM that revealed three loci on chromosomes 4 (QTL4c1 = 0.9–5.2 Mb, QTL4c2 = 6.9–15.7 Mb) and 5 (QTL5c = 18.3–24.1 Mb) (Figure 4C; Table S13). The genomic regions of QTL4c1 and QTL5c overlap with the HopAM1-induced cell death QTL4 (0.0–5.79 Mb) and QTL5A (16.3–21.3 Mb), but the most significant chlorosis locus, QTL4c2, was distinct from all QTL identified for HopAM1-induced cell death.

HopAM1-induced cell death and meristem chlorosis traits are independent among wild accessions

We also performed GWA mapping for HopAM1-induced meristem chlorosis among the 64 accessions that we had screened for HopAM1-induced cell death (see Table S11). The narrow sense heritability for the GWA study was $h^2 = 20.9\%$ (likelihood-ratio test, $P = 0.625$) and the most significant SNPs tended to have low minor allele frequencies (see Figure S6B). There was an enrichment of the most significantly associated SNPs with QTL4C2 (Table 2). However, the only peak above the stringent Bonferroni significance level was outside of the QTL intervals (Figure 5). This SNP and 3 more of the 10 most significant meristem chlorosis SNPs (FDR ≤ 0.05; including the top hit) fell within a 235-bp region between the third and fourth exon of *TOC64-III* (At3g17970), which encodes a protein of the chloroplast outer envelope membrane transport complex (see Table S14) (Sommer *et al.* 2013). In total, 27 out of the 50 top hits fell within a 2-kb region of *TOC64-III* (third to ninth exon). Alignment of all the 1001 Genomes haplotypes that were used in the GWA study across a 30-kb region spanning the top SNP indicated a correlation between *TOC64-III* haplotype and HopAM1-induced meristem chlorosis response (see Figure S9 and File S2). Single *toc64-III* mutants, and a *toc64* triple mutant (see *Materials and Methods*) were tested in the background of the meristem chlorosis-responsive accession Col-0. All *toc64* mutants, including the triple mutant, were responsive for HopAM1-induced meristem chlorosis, indicating that lack of TOC64 is not sufficient to prevent the effect.

We also screened additional *Arabidopsis* mutants for lack of HopAM1-induced meristem chlorosis (see Table S15). The double mutant *rbohd rbohf* (CS68522) (Torres *et al.* 2002) was not responsive, suggesting that superoxide derived from this NADPH oxidase complex is required for the phenotype. Both *eds1-2* and an *ein2-1 pad4-1 sid2-2* (CS66006) triple mutant enhanced the meristem chlorosis by extending the duration of time in which plants produced chlorotic leaves compared to controls (see Figure S10). Neither the *ein2-1 sid2-2* double mutant nor *pad4-1* exhibited this enhanced chlorosis. EDS1 and PAD4 proteins interact and potentiate accumulation of salicylic acid (SA) in pathogen-infected tissues, potentially through regulation of TIR-NLR action (Feys *et al.* 2001; Rietz *et al.* 2011; Wagner *et al.* 2013). *SID2* encodes isochorismate synthase 1 (ICS1) required for production of SA (Wildermuth *et al.* 2001). The extended chlorosis response of these two mutant lines suggests HopAM1 chlorosis is limited in timing through EDS1 function. All other Col-0 background mutant lines were similar to the parental Col-0 accession.

Host transcriptional signatures indicate that HopAM1 suppresses MTI but also induces ETI in Bur-0

To further investigate how HopAM1 interferes with host cellular functions, we performed genome-wide transcriptome analysis of infected plants. Col-0 and Bur-0 plants that were 5 weeks old were hand inoculated with *Pto* DC3000D28E(EV) or *Pto* DC3000D28E(*hopAM1*). RNA-seq libraries were prepared from plants harvested immediately before infiltration and at six time points postinfiltration spanning a 12 hr period (see *Materials and Methods*). The number of differentially expressed genes between plants inoculated with *Pto* DC3000D28E(EV) and *Pto* DC3000D28E(*hopAM1*) was relatively low at 2 hpi, a time point just preceding delivery of type III effectors (de Torres Zabala *et al.* 2009), for both

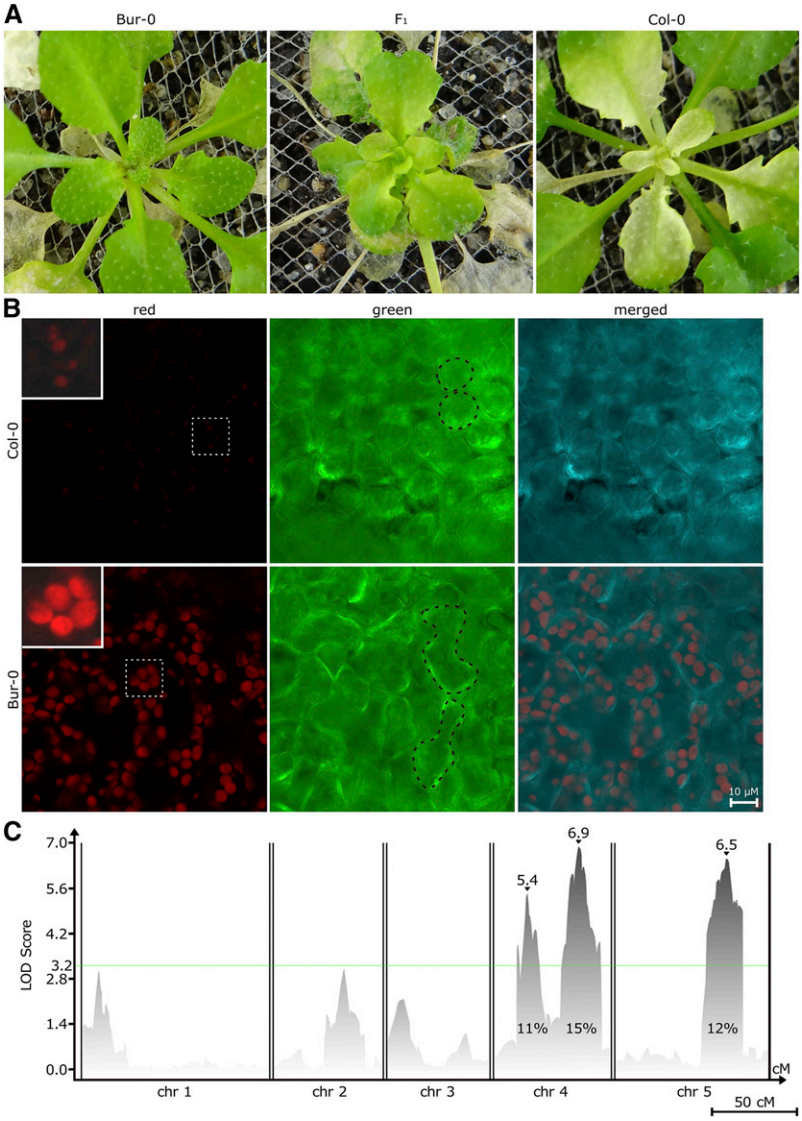

Figure 4 HopAM1 induces rosette chlorosis affecting chloroplast development and cell morphology controlled by three QTL in Col-0 × Bur-0. (A) Meristem chlorosis response following bacterial vacuum infiltration with *Pto* DC3000D28E(*hopAM1*). Col-0 exhibits strong chlorosis symptoms, while Bur-0 does not. F_1 progeny exhibit mild symptoms. Chlorosis appears in newly emerging leaf and meristem in Col-0 at 10 dpi following vacuum infiltration. Chlorosis can be observed up to 21 dpi. (B) Confocal laser scanning microscopy of *Arabidopsis* accessions Col-0 and Bur-0 leaf tissue, harvested 14 dpi following vacuum infiltration with *Pto* DC3000D28E(*hopAM1*). Chlorophyll autofluorescence (enlarged and brightened insets with white dotted outline shown on the top left corner of respective panel) (red channel), plant cell shape (black dotted outline of cells) (green channel), and merged channels are shown for each accession. Upper and lower panels taken at equal light intensity. Bar, 10 µm. (C) CIM on 342 reannotated RILs from a Col-0 × Bur-0 collection. The *x*-axis displays chromosomes 1 through 5 with map distances in cM. Peak LOD scores are shown by ▼ along with their values. Effects on phenotype variation are shown as percentages for all three QTL. The global permutation level of significance was set on LOD 3.2. Bar, 50 cM.

accessions (306 in Col-0 and only 4 in Bur-0; Figure 6A). The number of differentially expressed genes greatly increased over the remainder of the infection time course, ranging from 1432 to 2981 in Col-0 and from 522 to 5762 in Bur-0 (Figure 6A). The complete edgeR results are presented in Table S16. HopAM1-dependent differential expression was minimal for the 10 most highly associated loci identified in each GWA study. The HopAM1 chlorosis QTL regions still include hundreds of genes and many of them showed HopAM1-dependent transcriptional responses at some time points. The more narrowly defined cell death related QTL, QTL4, QTL5A, and QTL5B, also included multiple genes with differential expression in response to HopAM1 (see Table S7).

GO-enrichment analyses showed that HopAM1 downregulated defense-related genes at most time points in Col-0, and at the early time points in Bur-0 (see Figure S11; Table S17, Table S18, Table S19, Table S20, and Table S21). We determined if the changes in expression of defense-responsive genes were related to MTI or ETI by focusing on the expression of 1418 genes induced by the well-characterized MAMP flg22 (Rallapalli *et al.* 2014) for MTI and for ETI, on expression profiles of a set of 747 markers corresponding to genes upregulated in a comparison of Col-0 plants infected with ETI-inducing *Pto* DC3000(*avrRps4*) (triggering the RPS4 TIR-NLR) *vs.* plants infected with virulent *Pto* DC3000 (Howard *et al.* 2013). The average expression profile of the flg22-induced genes after infection with *Pto* DC3000(*hopAM1*) compared to Pto DC3000(EV) is consistent with HopAM1 suppressing MTI in both accessions at early time points. At 10–12 hpi, ETI-induced genes were upregulated by HopAM1 in Bur-0 but not in Col-0 (Figure 6B). Specific genes associated with typical immune responses such as *GSL5* (At4g03550), *RBOHD* (At5g47910), *SAG101* (At5g14930), *NDR1* (At3g20600), and *SID2* (At1g74710) were upregulated in Bur-0 from 10 hpi onwards, but not in Col-0 (see Figure S12). Our gene expression profiling indicates that HopAM1 induces an ETI response in the Bur-0 accession, which supports rapid HopAM1-induced cell death;

Table 2 P-values of enrichment tests of increasing numbers of most significant SNPs for each HopAM1-induced chlorosis QTL

Number of top SNPS	10	50	100	500	1000	10000
QTL4C1	1	0.982	0.959	0.93	0.502	0.993
QTL4C2	0.114	0.0253	0.0145	0.0006	0.0002	0.0002
QTL5C	0.898	0.999	1	07.93×10^{-01}	1	1

Calculated as in Table 1.

but not in Col-0, which does not. Notably, this difference in ETI response is not correlated with restriction of bacterial growth in Bur-0 compared to Col-0 (Figure 3).

P. syringae type III effectors suppress MTI transcriptional responses in the host plant (Truman *et al.* 2007; Lewis *et al.* 2015). Since HopAM1 is delivered to host plants by *Pto* DC3000 along with the rest of its suite of type III effectors, we expected that the transcriptional response to infection with *Pto* DC3000 should overlap with the response to Pto DC3000D28E(*hopAM1*). Lewis *et al.* (2015) identified a set of 2325 *Arabidopsis* genes that were differentially expressed (769 downregulated, 1556 upregulated) during the infection with *Pto* DC3000, but not with the mutant *Pto* DC3000*hrpA*. Since the *hrpA* mutant does not deliver effectors into the host cells, the differential gene expression was dependent on the bacterial effectors of *Pto* DC3000. A total of 213 of the 769 *Pto* DC3000 effector downregulated genes (28%) were also downregulated by HopAM1. These genes were enriched in biological processes related to nucleosome organization and chromatin assembly (FDR < 0.001; see Table S22). Furthermore, 510 of the 1556 genes (33%) activated by *Pto* DC3000 effectors were also upregulated by HopAM1 in our experiment. These genes were enriched in biological processes related to autophagy and photoperiodism (FDR < 0.001; see Table S22). MAMP perception has been shown to trigger large-scale suppression of genes for chloroplast-localized proteins in *Arabidopsis*, but that suppression was attenuated in plants infected with *Pto* DC3000, due to the combined functions of its collection of type III effectors (de Torres Zabala *et al.* 2015). When compared to *Pto* DC3000D28E(EV), infection with *Pto* DC3000D28E(*hopAM1*) resulted in higher expression of genes encoding chloroplast-localized proteins in both Col-0 and Bur-0 at 4 and 6 hpi, followed by reduced expression in both accessions by 12 hpi (see Figure S13); indicating that HopAM1 may affect chloroplast responses to MTI (Figure 4B) in both accessions even though Bur-0 does not suffer from meristem chlorosis.

Discussion

HopAM1-induced local cell death is associated with HopAM1-induction of ETI response

Using RNA-seq, we compared gene expression changes induced by *Pto* DC3000D28E(*hopAM1*) to changes induced by *Pto* DC3000D28E(EV). We found that HopAM1 repressed gene sets related to MTI immune responses in both Col-0 and Bur-0 at early time points (Figure 6B). Our results are consistent with our previous report that HopAM1 suppresses basal defense responses (Goel *et al.* 2008). Genes suppressed by HopAM1 overlapped with genes suppressed by *Pto* DC3000 delivering its full suite of type III effectors that includes HopAM1 (Truman *et al.* 2007; de Torres Zabala *et al.* 2015; Lewis *et al.* 2015). However, at 10–12 hpi, we defined a Bur-0-specific induction of genes previously associated with RPS4-dependent ETI (Howard *et al.* 2013) (Figure 6C; see Figure S11). As expected, if the early onset cell death seen in Bur-0 is the result of induced ETI, it is attenuated in F_2 plants from crosses of Bur-0 with Col-0-derived mutants that were homozygous for loss-of-function mutations in *HSP90.2* and *SGT1b* (Figure 1E) required for NLR receptor activation (Hubert *et al.* 2003; Holt *et al.* 2005; Shirasu 2009).

Our QTL analysis for HopAM1-induced cell death on the Bur-0 $\times$ Col-0 RIL population revealed multiple loci contributing additively to the timing of onset of cell death (Figure 1D). The three loci that account for most of the variation (QTL4, QTL5A, and QTL5B) each contain genes encoding NLR proteins, ETI receptors that are often highly variable in *Arabidopsis* (Shen *et al.* 2006; Cui *et al.* 2015) (see Table S3 and Table S7). Additional fine mapping and mutation analysis of individual candidates will be necessary to confirm candidate genes as responsible for the QTL traits. Specific alleles at each of the cell death QTL loci contribute additively to induce cell death earlier in Bur-0 than in other accessions as if each locus has an independent ETI function and the timing of cell death depends on the accumulation of effects from each locus. This is unlike the well-characterized ETI responses to pathogen effector proteins that present as gene-for-gene resistance scenarios, where one NLR gene is sufficient to mount an effective ETI response when its product recognizes the action of one type III effector (Dangl and Jones 2001).

GWA studies complement QTL mapping in biparental populations

Since they work at the population level, GWA studies have maximal power to detect associations with common allele variants and might give additional clues to understand species-wide adaptation patterns. GWA studies can identify loci even when they have relatively low power (Atwell *et al.* 2010) or when heritability is apparently low (Fournier-Level *et al.* 2011), and provide much higher mapping resolution with fewer individuals than QTL analysis (Balasubramanian *et al.* 2009). Successful examples are GWA studies of plant fitness in field experiments in which a myriad of causal loci with environmental-dependent effects lowered heritability estimates below 50%, usually closer to zero, but loci underlying relevant ecological traits were still found (Fournier-Level *et al.* 2011; Fournier-Level *et al.* 2013). In humans, GWA with polygenic and complex disease traits such as human height or schizophrenia keep providing new gene candidates and promote advances in quantitative genetic theory (Eichler *et al.* 2010; Visscher *et al.* 2010; Yang *et al.* 2010; Lee

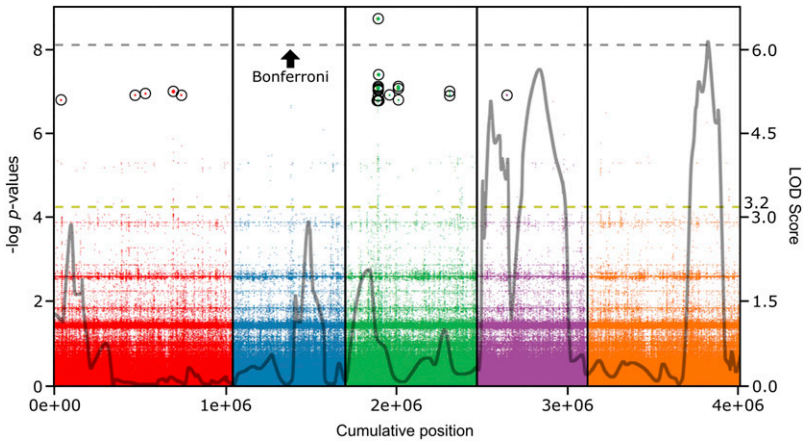

Figure 5 The genetic architecture of the HopAM1 chlorosis response defined by GWA is associated with a single locus on chromosome 3. HopAM1-induced chlorosis was scored in a collection of 64 *Arabidopsis* accessions as for Figure 2. Nearly all top 10 hits were inside genes. Gray outline reprises the QTL regions identified in Figure 4C in the Bur-0 × Col-0 background (cM converted to Mb only for each genetic marker's coordinates on the genome and shows LOD score at that specific location; not identical, but very similar to peak LOD scores shown in previous QTL analysis in Figure 4C). Right *y*-axis, LOD score; yellow-dotted line, significance threshold for CIM.

et al. 2014). The most significant candidate genes from our HopAM1-induced cell death GWA have functions consistent with affecting an ETI response. The most significantly associated SNPs were in the gene for cyclophilin 40, involved in epigenetic gene regulation, which is important to most cellular functions and certainly relevant to mounting effective ETI responses (Navarro *et al.* 2006; Zhai *et al.* 2011; Shivaprasad *et al.* 2012). Other significant cell death SNPs were located between a gene for brassinosteroid synthesis (*STEROL Δ-7 REDUCTASE*) and a gene for regulation of gibberellic acid signaling (*SCL3*). Both hormones contribute to the interplay of plant hormones that balances plant growth and defense (Bari and Jones 2009; Lozano-Duran and Zipfel 2015).

Local cell death is associated with activation of ETI responses even though it is not linked to changes in pathogen growth

The HopAM1-induced ETI response does not result in less growth of *Pto* DC3000 in Bur-0 than in Col-0 (Figure 3). Thus, while there is a clear ETI transcriptional signature from HopAM1 in Bur-0 that is cell death related, this ETI signature is decoupled from growth restriction itself. There are several examples of NLR-mediated ETI in which cell death and pathogen growth are uncoupled (reviewed in Coll *et al.* 2011), such as the extreme resistance to potato virus X by the Rx NLR protein (Bendahmane *et al.* 1999). Some ecotypes of *Arabidopsis* are resistant to *P. syringae* encoding the type III effectors AvrRps4 or HopA1 without developing obvious local lesions (Gassmann 2005; Kim *et al.* 2009). Uncoupling of effector-triggered cell death and pathogen growth restriction has also been observed for a number of *Arabidopsis* mutants such as cyclic nucleotide gated ion channel mutants *dnd1* (Clough *et al.* 2000), *hlm1* (Balague *et al.* 2003), *dnd2* (Jurkowski *et al.* 2004), and *metacaspase 1* (Coll *et al.* 2010). The extent of cell death can also vary depending on physiological conditions, such as light (Zeier *et al.* 2004; Bruggeman *et al.* 2015) and temperature (Menna *et al.* 2015) without loss of bacterial growth restriction.

A further hint that HopAM1 targets NLR-dependent downstream pathways comes from results showing that *EDS1* plays a role both in HopAM1-induced cell death (Figure 1E) and meristem chlorosis (see Figure S10). In most examples, *eds1* loss-of-function mutants cause reduction in pathogen- or stress-induced TIR-NLR-mediated ETI and cell death responses (Bartsch *et al.* 2006; Ochsenbein *et al.* 2006; Bhattacharjee *et al.* 2011). Interestingly, HopAM1 induced a constant transcriptional upregulation in Col-0 and Bur-0 from 6 hpi of both *EDS1* (At3g48090) and *PAD4* (At3g52430) (see Table S16). However, if HopAM1-mediated cell death is the consequence of ETI activation of a TIR-NLR, a loss-of-function mutant like *eds1-2* is expected to be unable to mount the ETI response. Instead, homozygosity for the *eds1-2* allele enhanced cell death in our F_2 plants (Figure 1E). Such a counterintuitive observation of a loss-of-function *eds1* mutation resulting in stronger NLR-mediated cell death has been observed before: the *eds1-2* mutation has been shown to enhance the immune response of an autoactive mutant derived from the CC-NLR gene *ADR1* (Roberts *et al.* 2013). In this regard, our finding of a cluster of CC-NLR genes in QTL5B, which we reduced to an interval of 100 kb containing only 30 genes, may suggest that one or more of these genes is causally related to HopAM1-induced cell death in Bur-0. Further fine mapping will address this possibility.

HopAM1 may reduce MTI responses through changes in chloroplast metabolism

Reactive oxygen, specifically superoxide, is required for HopAM1-induced meristem chlorosis since the double mutant of *RBOHD* and *RBOHF* did not support it (see Figure S10). Reactive oxygen species (ROS) accumulation is an integral part of MTI and ETI responses and high levels of ROS damage chloroplasts (Wagner *et al.* 2004; Kim *et al.* 2012). Chloroplasts play a key role in defense by producing ROS (Shapiguzov *et al.* 2012) and balancing hormone levels (Robert-Seilaniantz *et al.* 2011), thus constituting a target of preference for pathogens. *Pto* DC3000 effectors can suppress the expression of nuclear-encoded chloroplast genes in *Arabidopsis* and target the chloroplast (de Torres Zabala *et al.* 2015). Our expression analyses demonstrate that HopAM1 modifies the transcription of genes for chloroplast-localized proteins (see Figure S13). Our GWA study identified *TOC64III*, as significantly associated with variation in

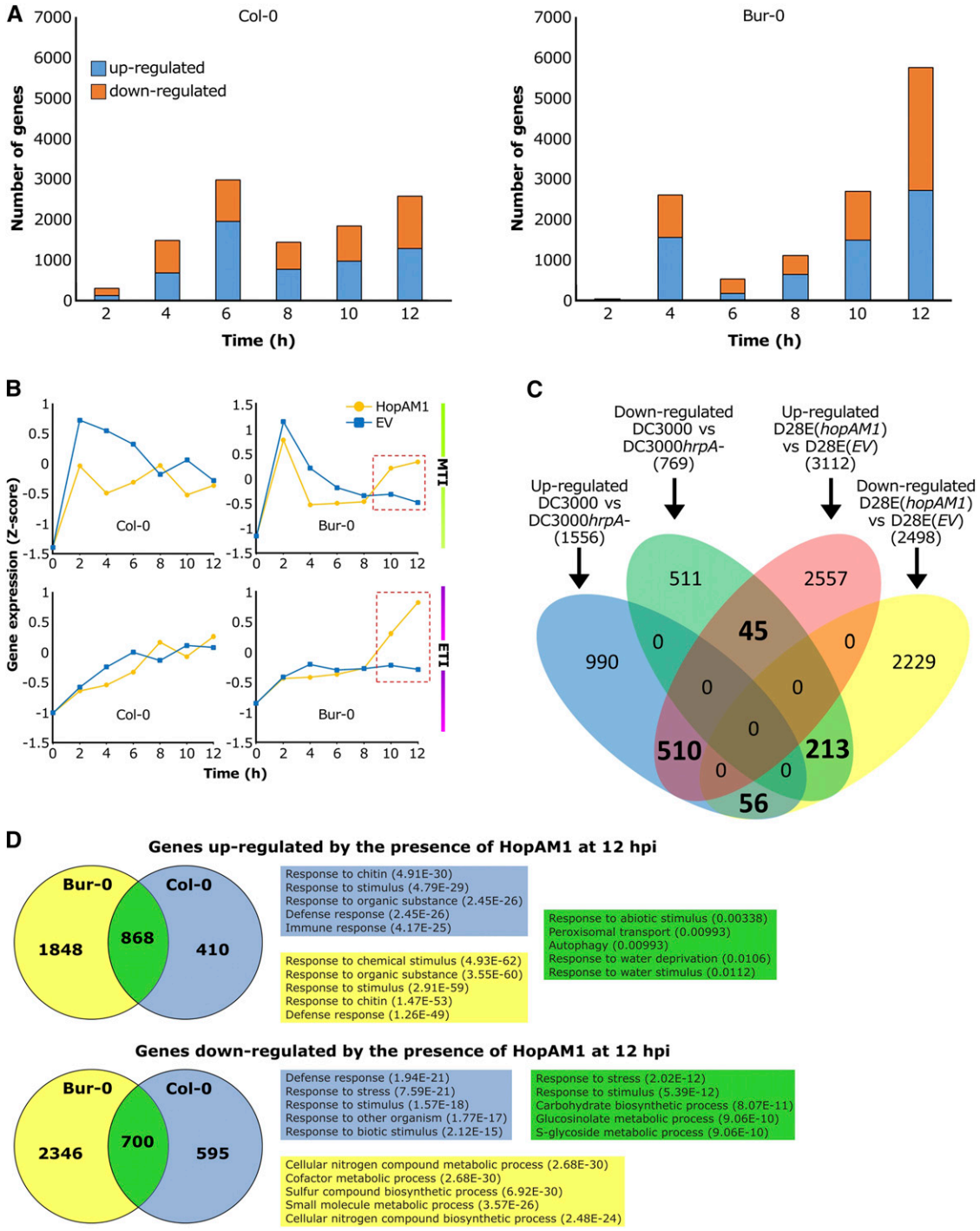

Figure 6 HopAM1 induces intense transcriptional reprogramming for thousands of genes in Col-0 and Bur-0, results in initial suppression of MTI in both ecotypes and later induction of ETI in Bur-0 only. (A) Number of genes (*y*-axis) differentially expressed as a result of HopAM1 delivery in Col-0 and Bur-0 every 2 hr (*x*-axis) in the first 12 hr postinfiltration. Orange bar, downregulated; blue bar, upregulated. (B) Upper panel: average expression profile of flg22-induced genes within the same time period in Col-0 and Bur-0. Lower panel: average expression profile of genes upregulated by ETI induced upon recognition of the avrRps4 avirulence factor by the NLR protein Rps4 in Col-0. Gene expression is shown as the median z-scored transformed RPKM values of the 1418 and 718 marker genes for MTI and ETI, respectively. (C) Overlap between genes differentially expressed by *Pto* DC3000D28E (*hopAM1*) infection and those specifically misregulated by *Pto* DC3000 effectors. A total of 5610 genes that were differentially expressed in Col-0 in at least one time point of our experiment were included in the analysis. A set of 517 genes showing ambiguous regulation (*i.e.*, both up- and down-regulation at different time points) was discarded. (D) Venn diagrams showing number of genes upregulated and downregulated at 12 hpi for both Bur-0 and Col-0. GOs for the top five sets are shown for each group.

chlorosis phenotype (Figure 4; Table S14). *TOC64III* encodes a chloroplast TOC transporter accessory protein (Sohrt and Soll 2000; Aronsson *et al.* 2007) which modulates the translocation efficiency of proteins into the chloroplast (Sommer *et al.* 2013). TOC64 protein is not essential for chloroplast function; no detrimental phenotype is observed under standard growth conditions for *Arabidopsis* insertion mutants defective in *TOC64III*. (Aronsson *et al.* 2007). Likewise, TOC64 protein is not necessary for response to HopAM1 although allelic variation is associated with different chlorotic responses to HopAM1. We suggest that allelic variation in TOC64 could render chloroplasts more or less resistant to damage caused by ROS induced during MTI defense responses.

Do meristem chlorosis and HopAM1 local cell death share a common mechanism?

HopAM1-induced local cell death and meristem chlorosis are not mutually exclusive. Both early cell death and chlorosis were observed in the Hov-4 and Wil-2 accessions (see Figure S7 File S1). Nevertheless, two of the three QTL loci related to meristem chlorosis from the Bur-0 × Col-0 RIL population overlap. Until the genes responsible for each phenotype have been identified, it is possible that independent genes and independent processes are responsible for chlorosis or cell death. However, the fact that *eds1-2* mutants both enhance cell death and meristem chlorosis suggests that EDS1 is a negative regulator of both HopAM1 responses. EDS1 regulates cell death by balancing phytohormone levels that lead to enhanced ROS production, likely involving modulation of TIR-NLR activation (Wiermer *et al.* 2005; Ochsenbein *et al.* 2006; Muhlenbock *et al.* 2008; Kim *et al.* 2012). Although our QTL and GWA analysis showed that HopAM1-induced chlorosis and cell death require distinct loci, *EDS1* appears to play an integral role in a critical biochemical junction where these two responses converge.

Conclusions

Pathogen effectors interact with and alter components of protein complexes important to plant immunity (Mukhtar *et al.* 2011; Weßling *et al.* 2014; Macho and Zipfel 2015). Therefore, individual pathogen effector proteins can serve as probes to identify interacting partners in immune complexes. To our knowledge, this is the first time that responses to a single pathogen effector have generated quantitative trait responses in the host. Previously defined ETI-related gene transcriptional alterations were also not associated with HopAM1-dependent bacterial growth restriction, which challenges the concept of what constitutes an ETI response, and more importantly, what is required to halt pathogen proliferation. Our study demonstrates that dissection of natural variation of host plants for quantitative responses to individual effectors, such as HopAM1, can reveal multiple genes involved in plant immune responses and help to dissect the quantitative features of what is often assumed to be a qualitative response.

Acknowledgments

We thank Marc Nishimura for immeasurable assistance with materials and advice. We also thank Farid El Kasmi, Eui-Hwan Chung, Freddy Monteiro, Scott Yourstone, and Sur Herrera-Paredes for general assistance and advice; and Joseph Kieber, Jason Reed, Li Yang, Christine Camilleri, Salomé Prat, and Úrsula Flores Pérez for providing various mutant lines used in this study. M.I., M.G.C., C.-M.V., T.D., and S.R.G. were supported by National Science Foundation grant IOS-1022286. Work at the Max Planck Institute was supported by Energy Regulatory Commission Advanced Grant IMMUNEMESIS. J.L.D. is an investigator of the Howard Hughes Medical Institute (HHMI), supported by the HHMI and the Gordon and Betty Moore Foundation (GBMF3030) and was also supported by National Science Foundation grant IOS-1257373. P.J.P.L.T. was supported by a fellowship from the Pew Latin American Fellows Program in the Biomedical Sciences.

Literature Cited

1001 Genomes Project Consortium, 2016 1,135 genomes reveal the global pattern of polymorphism in *Arabidopsis thaliana*. Cell 166: 481–491.

Anders, S., P. T. Pyl, and W. Huber, 2015 HTSeq—a Python framework to work with high-throughput sequencing data. Bioinformatics 31: 166–169.

Arnold, D. L., R. W. Jackson, A. J. Fillingham, S. C. Goss, J. D. Taylor *et al.*, 2001 Highly conserved sequences flank avirulence genes: isolation of novel avirulence genes from *Pseudomonas syringae* pv. *pisi*. Microbiology 147: 1171–1182.

Aronsson, H., P. Boij, R. Patel, A. Wardle, M. Töpel *et al.*, 2007 Toc64/OEP64 is not essential for the efficient import of proteins into chloroplasts in *Arabidopsis thaliana*. Plant J. 52: 53–68.

Atwell, S., Y. S. Huang, B. J. Vilhjálmsson, G. Willems, M. Horton *et al.*, 2010 Genome-wide association study of 107 phenotypes in a common set of *Arabidopsis thaliana* inbred lines. Nature 465: 627–631.

Austin, M. J., P. Muskett, K. Kahn, B. J. Feys, J. D. G. Jones *et al.*, 2002 Regulatory role of SGT1 in early R gene-mediated plant defenses. Science 295: 2077–2080.

Balague, C., B. Lin, C. Alcon, G. Flottes, S. Malmstrom *et al.*, 2003 HLM1, an essential signaling component in the hypersensitive response, is a member of the cyclic nucleotide-gated channel ion channel family. Plant Cell 15: 365–379.

Balasubramanian, S., C. Schwartz, A. Singh, N. Warthmann, M. C. Kim *et al.*, 2009 QTL mapping in new *Arabidopsis thaliana* advanced intercross-recombinant inbred lines. PLoS One 4: e4318.

Baltrus, D. A., M. T. Nishimura, A. Romanchuk, J. H. Chang, M. S. Mukhtar *et al.*, 2011 Dynamic evolution of pathogenicity revealed by sequencing and comparative genomics of 19 *Pseudomonas syringae* isolates. PLoS Pathog. 7: e1002132.

Bari, R., and J. D. Jones, 2009 Role of plant hormones in plant defence responses. Plant Mol. Biol. 69: 473–488.

Bartsch, M., E. Gobbato, P. Bednarek, S. Debey, J. L. Schultze *et al.*, 2006 Salicylic acid–independent ENHANCED DISEASE SUSCEPTIBILITY1 signaling in *Arabidopsis* immunity and cell death is regulated by the monooxygenase *FMO1* and the Nudix hydrolase *NUDT7*. Plant Cell 18: 1038–1051.

Bendahmane, A., K. Kanyuka, and D. C. Baulcombe, 1999 The *Rx* gene from potato controls separate virus resistance and cell death responses. Plant Cell 11: 781–792.

Bhattacharjee, S., M. K. Halane, S. H. Kim, and W. Gassmann, 2011 Pathogen effectors target *Arabidopsis* EDS1 and alter its interactions with immune regulators. Science 334: 1405–1408.

Boch, J., V. Joardar, L. Gao, T. L. Robertson, M. Lim *et al.*, 2002 Identification of *Pseudomonas syringae* pv. *tomato* genes induced during infection of *Arabidopsis thaliana*. Mol. Microbiol. 44: 73–88.

Bonardi, V., and J. L. Dangl, 2012 How complex are intracellular immune receptor signaling complexes? Front. Plant Sci. 3: 237–246.

Boyes, D. C., J. Nam, and J. L. Dangl, 1998 The *Arabidopsis thaliana* RPM1 disease resistance gene product is a peripheral plasma membrane protein that is degraded coincident with the hypersensitive response. Proc. Natl. Acad. Sci. USA 95: 15849–15854.

Brady, S. M., M. Burow, W. Busch, Ö. Carlborg, K. J. Denby *et al.*, 2015 Reassess the *t* test: interact with all your data via ANOVA. Plant Cell 27: 2088–2094.

Bruggeman, Q., C. Raynaud, M. Benhamed, and M. Delarue, 2015 To die or not to die? Lessons from lesion mimic mutants. Front. Plant Sci. 6: 24–46.

Buell, C. R., V. Joardar, M. Lindeberg, J. Selengut, I. T. Paulsen *et al.*, 2003 The complete genome sequence of the *Arabidopsis* and tomato pathogen *Pseudomonas syringae* pv. *tomato* DC3000. Proc. Natl. Acad. Sci. USA 100: 10181–10186.

Century, K. S., E. B. Holub, and B. J. Staskawicz, 1995 *NDR1*, a locus of *Arabidopsis thaliana* that is required for disease resistance to both a bacterial and a fungal pathogen. Proc. Natl. Acad. Sci. USA 92: 6597–6601.

Chan, E. K. F., H. C. Rowe, J. A. Corwin, B. Joseph, and D. J. Kliebenstein, 2011 Combining genome-wide association mapping and transcriptional networks to identify novel genes controlling glucosinolates in *Arabidopsis thalian*a. PLoS Biol. 9: e1001125.

Chang, J. H., J. M. Urbach, T. F. Law, L. W. Arnold, A. Hu *et al.*, 2005 A high-throughput, near-saturating screen for type III effector genes from *Pseudomonas syringae*. Proc. Natl. Acad. Sci. USA 102: 2549–2554.

Chavigneau, H., N. Goue, S. Delaunay, A. Courtial, L. Jouanin *et al.*, 2012 QTL for floral stem lignin content and degradability in three recombinant inbred line (RIL) progenies of *Arabidopsis thaliana* and search for candidate genes involved in cell wall biosynthesis and degradability. Open J. Genetics 2: 7–30.

Cheng, H., L. Qin, S. Lee, X. Fu, D. E. Richards *et al.*, 2004 Gibberellin regulates *Arabidopsis* floral development via suppression of DELLA protein function. Development 131: 1055–1064.

Cheong, M. S., A. Kirik, J.-G. Kim, K. Frame, V. Kirik *et al.*, 2014 AvrBsT acetylates *Arabidopsis* ACIP1, a protein that associates with microtubules and is required for immunity. PLoS Pathog. 10: e1003952.

Chung, E.-H., L. da Cunha, A.-J. Wu, Z. Gao, K. Cherkis *et al.*, 2011 Specific threonine phosphorylation of a host target by two unrelated type III effectors activates a host innate immune receptor in plants. Cell Host Microbe 9: 125–136.

Clough, S. J., K. A. Fengler, I. C. Yu, B. Lippok, R. K. Smith, Jr. *et al.*, 2000 The *Arabidopsis dnd1* "*defense*, *no death*" gene encodes a mutated cyclic nucleotide-gated ion channel. Proc. Natl. Acad. Sci. USA 97: 9323–9328.

Coll, N. S., D. Vercammen, A. Smidler, C. Clover, F. Van Breusegem *et al.*, 2010 *Arabidopsis* type I metacaspases control cell death. Science 330: 1393–1397.

Coll, N. S., P. Epple, and J. L. Dangl, 2011 Programmed cell death in the plant immune system. Cell Death Differ. 18: 1247–1256.

Cournoyer, B., J. D. Sharp, A. Astuto, M. J. Gibbon, J. D. Taylor *et al.*, 1995 Molecular characterization of the *Pseudomonas syringae* pv. *pisi* plasmid-borne avirulence gene *avrPpiB* which matches the *R3* resistance locus in pea. Mol. Plant Microbe Interact. 8: 700–708.

Cui, H., K. Tsuda, and J. E. Parker, 2015 Effector-triggered immunity: from pathogen perception to robust defense. Annu. Rev. Plant Biol. 66: 487–511.

Cunnac, S., S. Chakravarthy, B. H. Kvitko, A. B. Russell, G. B. Martin *et al.*, 2011 Genetic disassembly and combinatorial reassembly identify a minimal functional repertoire of type III effectors in *Pseudomonas syringae*. Proc. Natl. Acad. Sci. USA 108: 2975–2980.

Dangl, J. L., and J. D. G. Jones, 2001 Plant pathogens and integrated defence responses to infection. Nature 411: 826–833.

Deslandes, L., and S. Rivas, 2012 Catch me if you can: bacterial effectors and plant targets. Trends Plant Sci. 17: 644–655.

de Torres Zabala, M., M. H. Bennett, W. H. Truman, and M. R. Grant, 2009 Antagonism between salicylic and abscisic acid reflects early host–pathogen conflict and moulds plant defence responses. Plant J. 59: 375–386.

de Torres Zabala, M., G. Littlejohn, S. Jayaraman, D. Studholme, T. Bailey *et al.*, 2015 Chloroplasts play a central role in plant defence and are targeted by pathogen effectors. Nature Plants 1: 15074.

Dodds, P. N., and J. P. Rathjen, 2010 Plant immunity: towards an integrated view of plant–pathogen interactions. Nat. Rev. Genet. 11: 539–548.

Eichler, E. E., J. Flint, G. Gibson, A. Kong, S. M. Leal *et al.*, 2010 Missing heritability and strategies for finding the underlying causes of complex disease. Nat. Rev. Genet. 11: 446–450.

Feys, B. J., L. J. Moisan, M.-A. Newman, and J. E. Parker, 2001 Direct interaction between the *Arabidopsis* disease resistance signaling proteins, EDS1 and PAD4. EMBO J. 20: 5400–5411.

Fournier-Level, A., A. Korte, M. D. Cooper, M. Nordborg, J. Schmitt *et al.*, 2011 A map of local adaptation in *Arabidopsis thaliana*. Science 334: 86–89.

Fournier-Level, A., A. M. Wilczek, M. D. Cooper, J. L. Roe, J. Anderson *et al.*, 2013 Paths to selection on life history loci in different natural environments across the native range of *Arabidopsis thaliana*. Mol. Ecol. 22: 3552–3566.

Fu, Z. Q., M. Guo, B.-r. Jeong, F. Tian, T. E. Elthon *et al.*, 2007 A type III effector ADP-ribosylates RNA-binding proteins and quells plant immunity. Nature 447: 284–288.

Gassmann, W., 2005 Natural variation in the *Arabidopsis* response to the avirulence gene *hopPsyA* uncouples the hypersensitive response from disease resistance. Mol. Plant Microbe Interact. 18: 1054–1060.

Gery, C., E. Zuther, E. Schulz, J. Legoupi, A. Chauveau *et al.*, 2011 Natural variation in the freezing tolerance of *Arabidopsis thaliana*: effects of RNAi-induced CBF depletion and QTL localisation vary among accessions. Plant Sci. 180: 12–23.

Gibson, G., 2012 Rare and common variants: twenty arguments. Nat. Rev. Genet. 13: 135–145.

Glazebrook, J., E. E. Rogers, and F. M. Ausubel, 1996 Isolation of *Arabidopsis* mutants with enhanced disease susceptibility by direct screening. Genetics 143: 973–982.

Goel, A. K., D. Lundberg, M. A. Torres, R. Matthews, C. Akimoto-Tomiyama *et al.*, 2008 The *Pseudomonas syringae* type III effector HopAM1 enhances virulence on water-stressed plants. Mol. Plant Microbe Interact. 21: 361–370.

Grant, J. J., A. Chini, D. Basu, and G. J. Loake, 2003 Targeted activation tagging of the *Arabidopsis* NBS-LRR gene, *ADR1*, conveys resistance to virulent pathogens. Mol. Plant Microbe Interact. 16: 669–680.

Holt, 3rd, B. F., D. C. Boyes, M. Ellerström, N. Siefers, A. Wiig *et al.*, 2002 An evolutionarily conserved mediator of plant disease

resistance gene function is required for normal *Arabidopsis* development. Dev. Cell 2: 807–817.
Holt, 3rd, B. F., Y. Belkhadir, and J. L. Dangl, 2005 Antagonistic control of disease resistance protein stability in the plant immune system. Science 309: 929–932.
Howard, B. E., Q. Hu, A. C. Babaoglu, M. Chandra, M. Borghi *et al.*, 2013 High-throughput RNA sequencing of *Pseudomonas*-infected *Arabidopsis* reveals hidden transcriptome complexity and novel splice variants. PLoS One 8: e74183.
Hubert, D. A., P. Tornero, Y. Belkhadir, P. Krishna, A. Takahashi *et al.*, 2003 Cytosolic HSP90 associates with and modulates the *Arabidopsis* RPM1 disease resistance protein. EMBO J. 22: 5679–5689.
Iki, T., M. Yoshikawa, T. Meshi, and M. Ishikawa, 2012 Cyclophilin 40 facilitates HSP90-mediated RISC assembly in plants. EMBO J. 31: 267–278.
Jones, J. D. G., and J. L. Dangl, 2006 The plant immune system. Nature 444: 323–329.
Joseph, B., J. A. Corwin, B. Li, S. Atwell, and D. J. Kliebenstein, 2013 Cytoplasmic genetic variation and extensive cytonuclear interactions influence natural variation in the metabolome. eLife 2: e00776.
Jurkowski, G. I., R. K. Smith, Jr., I. C. Yu, J. H. Ham, S. B. Sharma *et al.*, 2004 *Arabidopsis DND2*, a second cyclic nucleotide-gated ion channel gene for which mutation causes the "*defense, no death*" phenotype. Mol. Plant Microbe Interact. 17: 511–520.
Kang, H. M., J. H. Sul, S. K. Service, N. A. Zaitlen, S.-y. Kong *et al.*, 2010 Variance component model to account for sample structure in genome-wide association studies. Nat. Genet. 42: 348–354.
Kim, C., R. Meskauskiene, S. Zhang, K. P. Lee, M. Lakshmanan Ashok *et al.*, 2012 Chloroplasts of *Arabidopsis* are the source and a primary target of a plant-specific programmed cell death signaling pathway. Plant Cell 24: 3026–3039.
Kim, S. H., S. I. Kwon, D. Saha, N. C. Anyanwu, and W. Gassmann, 2009 Resistance to the *Pseudomonas syringae* effector HopA1 is governed by the TIR-NBS-LRR protein RPS6 and is enhanced by mutations in *SRFR1*. Plant Physiol. 150: 1723–1732.
Klimyuk, V. I., B. J. Carroll, C. M. Thomas, and J. D. G. Jones, 1993 Alkali treatment for rapid preparation of plant material for reliable PCR analysis. Plant J. 3: 493–494.
Kroj, T., E. Chanclud, C. Michel-Romiti, X. Grand, and J. B. Morel, 2016 Integration of decoy domains derived from protein targets of pathogen effectors into plant immune receptors is widespread. New Phytol. 210: 618–626.
Landgraf, A., H. Weingart, G. Tsiamis, and J. Boch, 2006 Different versions of *Pseudomonas syringae* pv. *tomato* DC3000 exist due to the activity of an effector transposon. Mol. Plant Pathol. 7: 355–364.
Lecain, E., X. Chenivesse, R. Spagnoli, and D. Pompon, 1996 Cloning by metabolic interference in yeast and enzymatic characterization of *Arabidopsis thaliana* sterol Δ7-reductase. J. Biol. Chem. 271: 10866–10873.
Lee, S., G. R. Abecasis, M. Boehnke, and X. Lin, 2014 Rare-variant association analysis: study designs and statistical tests. Am. J. Hum. Genet. 95: 5–23.
Lewis, L. A., K. Polanski, M. de Torres-Zabala, S. Jayaraman, L. Bowden *et al.*, 2015 Transcriptional dynamics driving MAMP-triggered immunity and pathogen effector-mediated immunosuppression in *Arabidopsis* leaves following infection with *Pseudomonas syringae* pv *tomato* DC3000. Plant Cell 27: 3038–3064.
Lincoln, S., M. Daly, and E. Lander, 1992 *Constructing genetic maps with MAPMAKER/EXP 3.0*. Whitehead Institute Technical Report. 3rd Edition. Whitehead Institute, Cambridge, MA.
Lozano-Duran, R., and C. Zipfel, 2015 Trade-off between growth and immunity: role of brassinosteroids. Trends Plant Sci. 20: 12–19.
Macho, A. P., and C. Zipfel, 2015 Targeting of plant pattern recognition receptor-triggered immunity by bacterial type-III secretion system effectors. Curr. Opin. Microbiol. 23: 14–22.
Menna, A., D. Nguyen, D. S. Guttman, and D. Desveaux, 2015 Elevated temperature differentially influences effector-triggered immunity outputs in *Arabidopsis*. Front. Plant Sci. 6: 995.
Muhlenbock, P., M. Szechynska-Hebda, M. Plaszczyca, M. Baudo, A. Mateo *et al.*, 2008 Chloroplast signaling and *LESION SIMULATING DISEASE1* regulate crosstalk between light acclimation and immunity in *Arabidopsis*. Plant Cell 20: 2339–2356.
Mukhtar, M. S., A. R. Carvunis, M. Dreze, P. Epple, J. Steinbrenner *et al.*, 2011 Independently evolved virulence effectors converge onto hubs in a plant immune system network. Science 333: 596–601.
Munkvold, K. R., M. E. Martin, P. A. Bronstein, and A. Collmer, 2008 A survey of the *Pseudomonas syringae* pv. *tomato* DC3000 type III secretion system effector repertoire reveals several effectors that are deleterious when expressed in *Saccharomyces cerevisiae*. Mol. Plant Microbe Interact. 21: 490–502.
Nagpal, P., L. M. Walker, J. C. Young, A. Sonawala, C. Timpte *et al.*, 2000 AXR2 encodes a member of the Aux/IAA protein family. Plant Physiol. 123: 563–574.
Navarro, L., P. Dunoyer, F. Jay, B. Arnold, N. Dharmasiri *et al.*, 2006 A plant miRNA contributes to antibacterial resistance by repressing auxin signaling. Science 312: 436–439.
Nordberg, H., M. Cantor, S. Dusheyko, S. Hua, A. Poliakov *et al.*, 2014 The genome portal of the Department of Energy Joint Genome Institute: 2014 updates. Nucleic Acids Res. 42: D26–D31.
Ochsenbein, C., D. Przybyla, A. Danon, F. Landgraf, C. Göbel *et al.*, 2006 The role of *EDS1* (enhanced disease susceptibility) during singlet oxygen-mediated stress responses of *Arabidopsis*. Plant J. 47: 445–456.
Rallapalli, G., E. M. Kemen, A. Robert-Seilaniantz, C. Segonzac, G. J. Etherington *et al.*, 2014 EXPRSS: an Illumina based high-throughput expression-profiling method to reveal transcriptional dynamics. BMC Genomics 15: 1–18.
Rietz, S., A. Stamm, S. Malonek, S. Wagner, D. Becker *et al.*, 2011 Different roles of Enhanced Disease Susceptibility1 (EDS1) bound to and dissociated from Phytoalexin Deficient4 (PAD4) in *Arabidopsis* immunity. New Phytol. 191: 107–119.
Roberts, M., S. Tang, A. Stallmann, J. L. Dangl, and V. Bonardi, 2013 Genetic requirements for signaling from an autoactive plant NB-LRR intracellular innate Immune receptor. PLoS Genet. 9: e1003465.
Robert-Seilaniantz, A., M. Grant, and J. D. Jones, 2011 Hormone crosstalk in plant disease and defense: more than just jasmonate-salicylate antagonism. Annu. Rev. Phytopathol. 49: 317–343.
Robinson, M. D., D. J. McCarthy, and G. K. Smyth, 2010 edgeR: a Bioconductor package for differential expression analysis of digital gene expression data. Bioinformatics 26: 139–140.
Romano, P., Z. He, and S. Luan, 2004 Introducing immunophilins. From organ transplantation to plant biology. Plant Physiol. 134: 1241–1243.
Schechter, L. M., M. Vencato, K. L. Jordan, S. E. Schneider, D. J. Schneider *et al.*, 2006 Multiple approaches to a complete inventory of *Pseudomonas syringae* pv. *Tomato* DC3000 type III secretion system effector proteins. Mol. Plant Microbe Interact. 19: 1180–1192.
Schneeberger, K., S. Ossowski, F. Ott, J. D. Klein, X. Wang *et al.*, 2011 Reference-guided assembly of four diverse *Arabidopsis thaliana* genomes. Proc. Natl. Acad. Sci. USA 108: 10249–10254.
Shapiguzov, A., J. P. Vainonen, M. Wrzaczek, and J. Kangasjarvi, 2012 ROS-talk – how the apoplast, the chloroplast, and the nucleus get the message through. Front. Plant Sci. 3: 292–301.
Shen, J., H. Araki, L. Chen, J.-Q. Chen, and D. Tian, 2006 Unique evolutionary mechanism in R-genes under the presence/absence

polymorphism in *Arabidopsis thaliana*. Genetics 172: 1243–1250.

Shirasu, K., 2009 The HSP90–SGT1 chaperone complex for NLR immune sensors. Annu. Rev. Plant Biol. 60: 139–164.

Shivaprasad, P. V., H. M. Chen, K. Patel, D. M. Bond, B. A. Santos *et al.*, 2012 A microRNA superfamily regulates nucleotide binding site-leucine-rich repeats and other mRNAs. Plant Cell 24: 859–874.

Simon, M., O. Loudet, S. Durand, A. Bérard, D. Brunel *et al.*, 2008 Quantitative trait loci mapping in five new large recombinant inbred line populations of *Arabidopsis thaliana* genotyped with consensus single-nucleotide polymorphism markers. Genetics 178: 2253–2264.

Smith, M. R., M. R. Willmann, G. Wu, T. Z. Berardini, B. Möller *et al.*, 2009 Cyclophilin 40 is required for microRNA activity in *Arabidopsis*. Proc. Natl. Acad. Sci. USA 106: 5424–5429.

Sohrt, K., and J. Soll, 2000 Toc64, a new component of the protein translocon of chloroplasts. J. Cell Biol. 148: 1213–1222.

Sommer, M., M. Rudolf, B. Tillmann, J. Tripp, M. S. Sommer *et al.*, 2013 Toc33 and Toc64-III cooperate in precursor protein import into the chloroplasts of *Arabidopsis thaliana*. Plant Cell Environ. 36: 970–983.

Tao, Y., Z. Xie, W. Chen, J. Glazebrook, H. S. Chang *et al.*, 2003 Quantitative nature of *Arabidopsis* responses during compatible and incompatible interactions with the bacterial pathogen *Pseudomonas syringae*. Plant Cell 15: 317–330.

Taylor, M. B., and I. M. Ehrenreich, 2014 Genetic interactions involving five or more genes contribute to a complex trait in yeast. PLoS Genet. 10: e1004324.

Thomas, W. J., C. A. Thireault, J. A. Kimbrel, and J. H. Chang, 2009 Recombineering and stable integration of the *Pseudomonas syringae* pv. *syringae* 61 hrp/hrc cluster into the genome of the soil bacterium *Pseudomonas fluorescens Pf0–1*. Plant J. 60: 919–928.

Tornero, P., P. Merritt, A. Sadanandom, K. Shirasu, R. W. Innes *et al.*, 2002 *RAR1* and *NDR1* contribute quantitatively to disease resistance in *Arabidopsis*, and their relative contributions are dependent on the *R* gene assayed. Plant Cell 14: 1005–1015.

Torres, M. A., J. L. Dangl, and J. D. G. Jones, 2002 *Arabidopsis* gp91phox homologues *AtrbohD* and *AtrbohF* are required for accumulation of reactive oxygen intermediates in the plant defense response. Proc. Natl. Acad. Sci. USA 99: 517–522.

Trapnell, C., L. Pachter, and S. L. Salzberg, 2009 TopHat: discovering splice junctions with RNA-Seq. Bioinformatics 25: 1105–1111.

Truman, W., M. H. Bennett, I. Kubigsteltig, C. Turnbull, and M. Grant, 2007 *Arabidopsis* systemic immunity uses conserved defense signaling pathways and is mediated by jasmonates. Proc. Natl. Acad. Sci. USA 104: 1075–1080.

van der Hoorn, R. A. L., and S. Kamoun, 2008 From guard to decoy: a new model for perception of plant pathogen effectors. Plant Cell 20: 2009–2017.

Visscher, P. M., B. McEvoy, and J. Yang, 2010 From Galton to GWAS: quantitative genetics of human height. Genet. Res. 92: 371–379.

Wagner, D., D. Przybyla, R. Op den Camp, C. Kim, F. Landgraf *et al.*, 2004 The genetic basis of singlet oxygen-induced stress responses of *Arabidopsis thaliana*. Science 306: 1183–1185.

Wagner, S., J. Stuttmann, S. Rietz, R. Guerois, E. Brunstein *et al.*, 2013 Structural basis for signaling by exclusive EDS1 heteromeric complexes with SAG101 or PAD4 in plant innate immunity. Cell Host Microbe 14: 619–630.

Wang, S., C. J. Basten, and Z.-B. Zeng, 2012 *Windows QTL Cartographer 2.5*. Department of Statistics, North Carolina State University, Raleigh, NC. Available at: http://statgen.ncsu.edu/qtlcart/WQTLCart.htm.

Wang, Y., C. Liu, K. Li, F. Sun, H. Hu *et al.*, 2007 *Arabidopsis* EIN2 modulates stress response through abscisic acid response pathway. Plant Mol. Biol. 64: 633–644.

Weigel, D., and M. Nordborg, 2015 Population genomics for understanding adaptation in wild plant species. Annu. Rev. Genet. 49: 315–338.

Weßling, R., P. Epple, S. Altmann, Y. He, and L. Yang *et al.*, 2014 Convergent targeting of a common host protein-network by pathogen effectors from three kingdoms of life. Cell Host Microbe 16: 364–375.

Wiermer, M., B. J. Feys, and J. E. Parker, 2005 Plant immunity: the EDS1 regulatory node. Curr. Opin. Plant Biol. 8: 383–389.

Wildermuth, M. C., J. Dewdney, G. Wu, and F. M. Ausubel, 2001 Isochorismate synthase is required to synthesize salicylic acid for plant defence. Nature 414: 562–565.

Wright, C. A., and G. A. Beattie, 2004 *Pseudomonas syringae* pv. *tomato* cells encounter inhibitory levels of water stress during the hypersensitive response of *Arabidopsis thaliana*. Proc. Natl. Acad. Sci. USA 101: 3269–3274.

Xin, X.-F., and S. Y. He, 2013 *Pseudomonas syringae* pv. *tomato* DC3000: a model pathogen for probing disease susceptibility and hormone signaling in plants. Annu. Rev. Phytopathol. 51: 473–498.

Yang, J., B. Benyamin, B. P. McEvoy, S. Gordon, A. K. Henders *et al.*, 2010 Common SNPs explain a large proportion of the heritability for human height. Nat. Genet. 42: 565–569.

Yi, X., Z. Du, and Z. Su, 2013 PlantGSEA: a gene set enrichment analysis toolkit for plant community. Nucleic Acids Res. 41: W98–W103.

Zeier, J., B. Pink, M. J. Mueller, and S. Berger, 2004 Light conditions influence specific defence responses in incompatible plant-pathogen interactions: uncoupling systemic resistance from salicylic acid and PR-1 accumulation. Planta 219: 673–683.

Zhai, J., D.-H. Jeong, E. De Paoli, S. Park, B. D. Rosen *et al.*, 2011 MicroRNAs as master regulators of the plant NB-LRR defense gene family via the production of phased, trans-acting siRNAs. Genes Dev. 25: 2540–2553.

Zhang, J., F. Shao, Y. Li, H. Cui, L. Chen *et al.*, 2007 A *Pseudomonas syringae* effector inactivates MAPKs to suppress PAMP-induced immunity in plants. Cell Host Microbe 1: 175–185.

Zhang, Z.-L., M. Ogawa, C. M. Fleet, R. Zentella, J. Hu *et al.*, 2011 SCARECROW-LIKE 3 promotes gibberellin signaling by antagonizing master growth repressor DELLA in *Arabidopsis*. Proc. Natl. Acad. Sci. USA 108: 2160–2165.

Zipfel, C., S. Robatzek, L. Navarro, E. J. Oakeley, J. D. G. Jones *et al.*, 2004 Bacterial disease resistance in *Arabidopsis* through flagellin perception. Nature 428: 764–767.

Zipfel, C., G. Kunze, D. Chinchilla, A. Caniard, J. D. Jones *et al.*, 2006 Perception of the bacterial PAMP EF-Tu by the receptor EFR restricts *Agrobacterium*-mediated transformation. Cell 125: 749–760.

Communicating editor: T. Juenger

GENETICS

Supporting Information
www.genetics.org/lookup/suppl/doi:10.1534/genetics.116.190678/-/DC1

Effector-Triggered Immune Response in *Arabidopsis thaliana* Is a Quantitative Trait

Michail Iakovidis, Paulo J. P. L. Teixeira, Moises Exposito-Alonso, Matthew G. Cowper, Theresa F. Law, Qingli Liu, Minh Chau Vu, Troy Minh Dang, Jason A. Corwin, Detlef Weigel, Jeffery L. Dangl, and Sarah R. Grant

DOI: 10.1534/genetics.116.190678

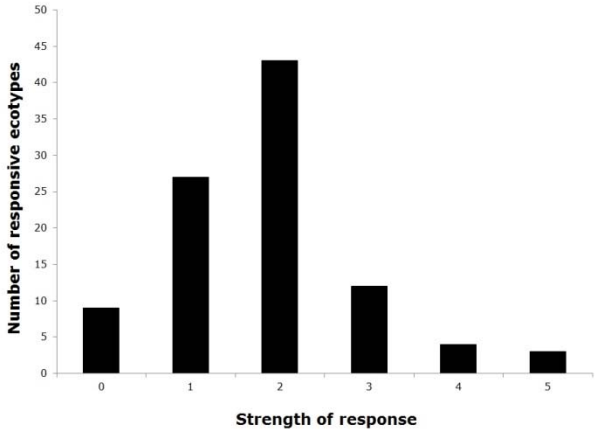

Figure S1 | Gaussian distribution of HopAM1-induced cell death phenotypic scores in *A. thaliana* germplasm. Chart showing a normal distribution observed across 98 accessions used in this study (Shapiro-Wilks Normality Test- W = 0.8877, *p-value* = 4.873e-07). Numbers of accessions in each phenotypic class based on the strength of the response (x-axis) are shown (y-axis).

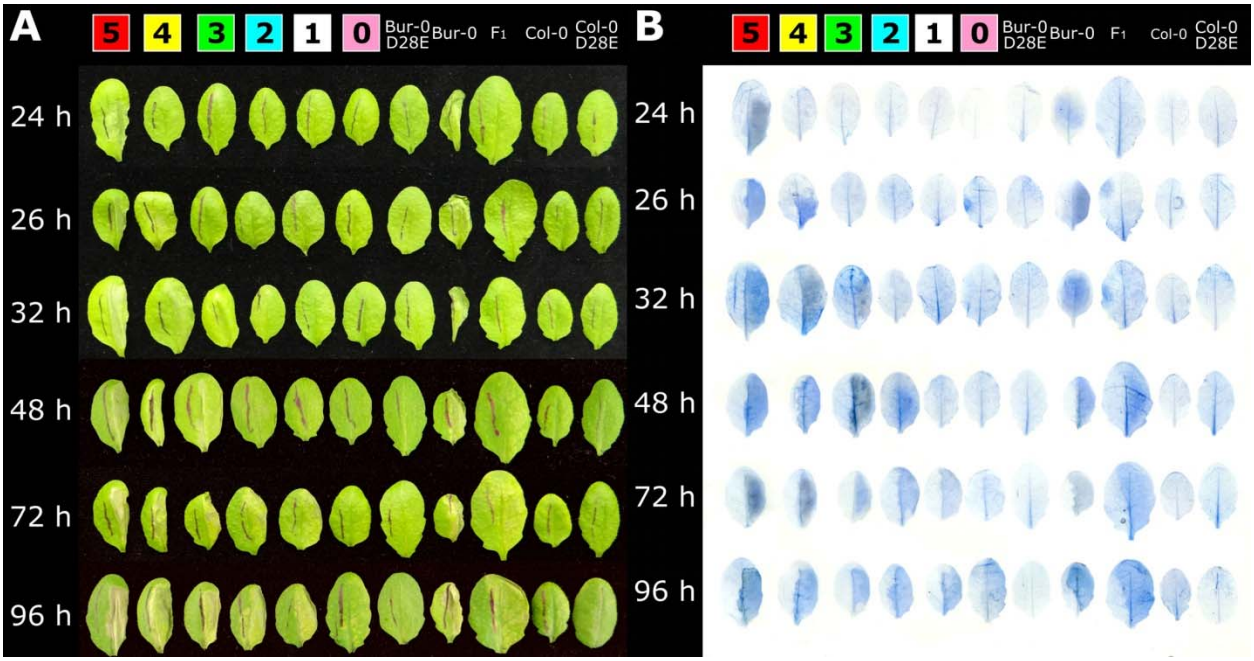

Figure S2 | HopAM1-induced cell death symptoms in Bur-0 x Col-0 RIL population. Visible cell death (A) and Trypan Blue stains (B) of selected RILs and controls for all time points used to phenotypically score the RIL population. The selected time points were chosen for practical reasons in order to quantify the phenotype. However, cell death symptoms continue to emerge throughout the 96 hour time window. All plants had 4 replicates. The leaves stained with Trypan Blue on the right are the same ones depicted on the left. Figure 1A-B is part of this image (Bur-0, F_1, Col-0; 48 hpi). All leaves were infiltrated with *Pto* DC3000D28E(*hopAM1*), except two negative controls (Bur-0 D28E and Col-0 D28E) that were infiltrated with *Pto* DC3000D28E.

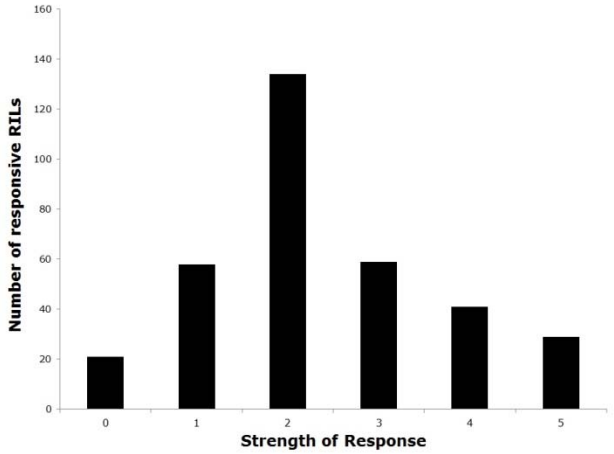

Figure S3 | Gaussian distribution of HopAM1-induced cell death phenotypic scores in Bur-0 x Col-0 RIL population. Chart showing a normal distribution observed across 324 RILs used in this study (Shapiro-Wilks Normality Test: W = 0.915, *p-value* = 5.52e-13).

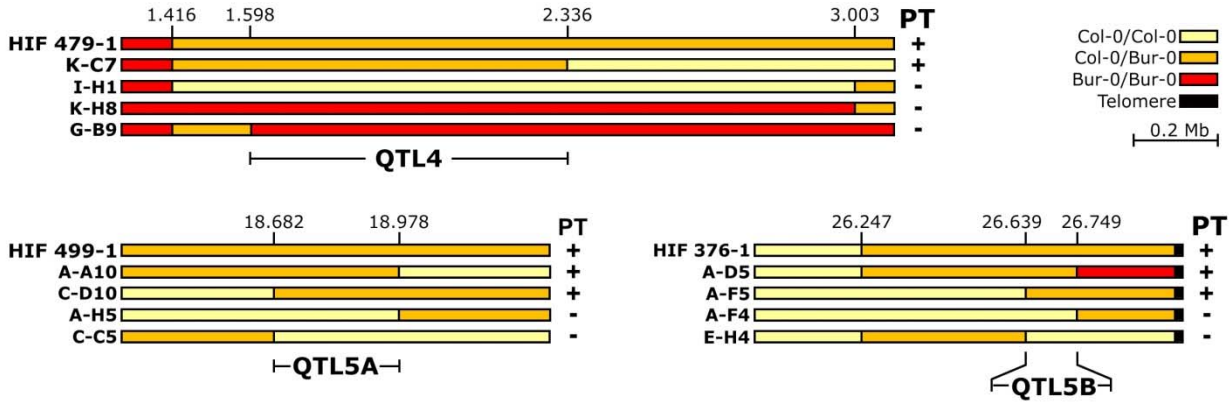

Figure S4 | Delimiting QTL intervals for fine mapping of HopAM1-induced cell death. Intervals for QTL4 on chromosome 4; QTL5A and QTL5B on chromosome 5. Progeny tests on HIFs 479-1, 499-1 and 376-1 showed that they were segregating for HopAM1-induced cell death and were chosen to fine map the respective QTLs. Progeny tests were used as the absolute measure to fine map the intervals as the heterozygous haplotype could attain any score (0-5) on the HopAM1-induced cell death response. A total of 2092 plants from HIF479-1 were genotyped for recombination events within a 1.587 Mb region of chromosome 4 (1.416 – 3.003 Mb) yielding six recombinant lines (0.3% recombination rate), which were progeny tested for HopAM1-induced cell death. The results narrowed the QTL4 interval to 738 kb between 1.598 and 2.336 Mb. For QTL5A, 768 plants from HIF376-1 were genotyped for recombination events within a 1.756 Mb region of chromosome 5 (18.360 – 20.116 Mb) yielding 107 recombinant lines (13.9% recombination rate). Following progeny testing on a subset of HIFs, the QTL5A interval was narrowed to a 296 kb region between 18.682 and 18.978 Mb. For QTL5B, 480 plants from HIF376-1 were genotyped for recombination events within a 1.142 Mb region of chromosome 5 (26.247 – 26.920 Mb) yielding 65 recombinant lines (13.7% recombination rate). Following progeny testing on a subset of HIFs, the QTL5B interval was narrowed to a 110 kb region between 26.639 and 26.749 Mb. Haplotype composition is shown on the chromosomal regions of interest (QTL4, QTL5A and QTL5B) for each HIF used for fine mapping. Distances are in megabases (Mb) and progeny tests (PT) for each line show whether they were segregating (+) or not (-) for HopAM1-induced cell death score (0-5).

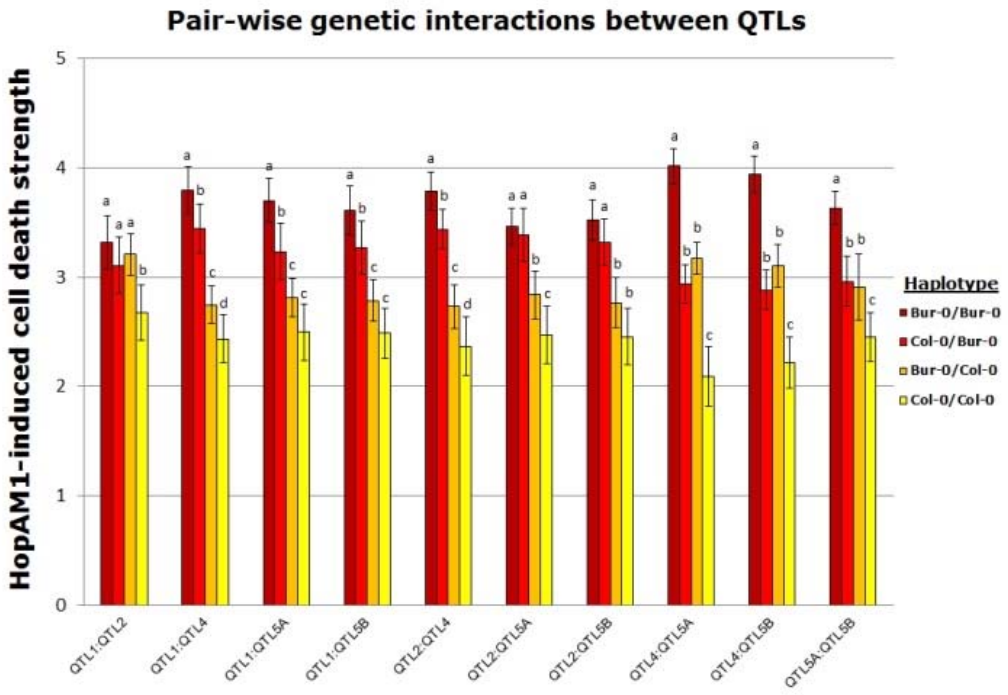

Figure S5 | QTLs in Bur-0 x Col-0 contribute additively to HopAM1-induced cell death. Allele contribution to the cell death phenotype in pair-wise comparison for all five QTLs. QTLs on chromosomes 4 and 5 appear to have the largest contribution to the phenotype. All interactions appear additive, non-epistatic. Bars show average phenotypic score for all RILs carrying the respective haplotype for each marker where LOD scores peaked at each QTL detected. Two times Standard Error values are shown as error bars. QTL haplotypes are color coded for the respective background of each QTL tested in each pair-wise comparison. Statistical significance is indicated by letters, based on pairwise *t*-tests ($P<0.05$).

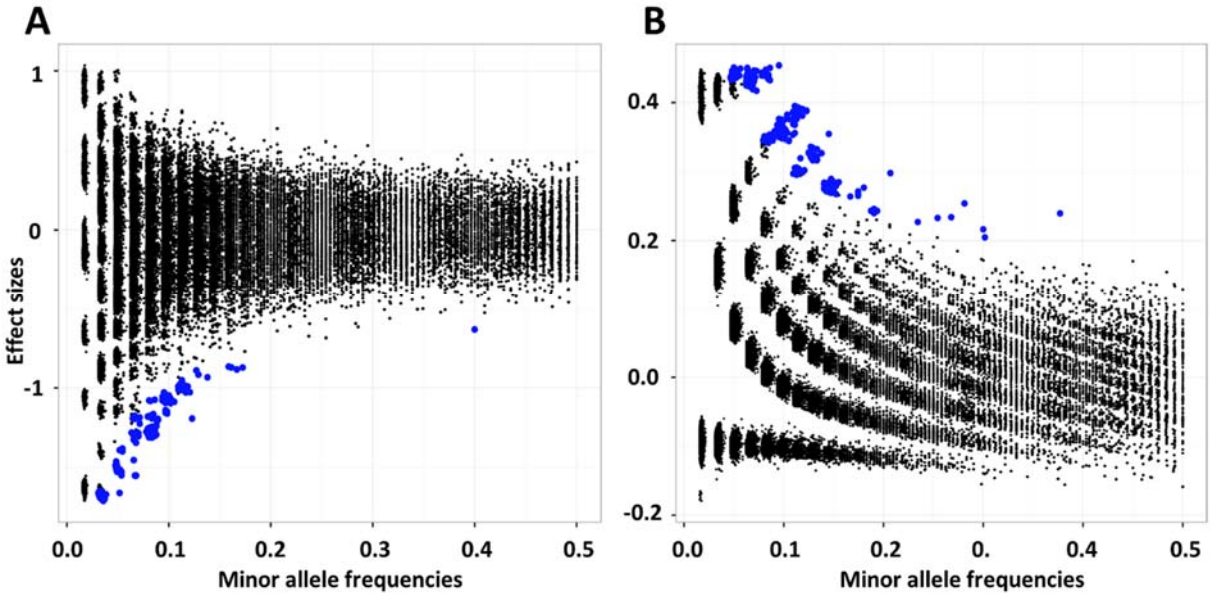

Figure S6 | Distribution of allele frequencies and effects for HopAM1-induced responses. Local cell death response (A) and HopAM1-induced meristem chlorosis response (B). Effect size represents standardized regression coefficients or “beta”. They are interpreted as the phenotypic difference between genotypes carrying the minor allele-frequency allele from those with the reference allele and are expressed in standard deviations of the phenotype. Each dot represents a tested SNP. The top 500 SNPs are in blue.

Figure S7 | Genomic alignment of accessions in relation to HopAM1-induced cell death response near the most significant SNP. *A. thaliana* sequence differences are shown spanning a 30 kb region on chromosome 3 from 6870000 to 6900000 bp, covering the area around the most significant SNP hit at 6879376 bp (shown by a yellow arrow). Sequence differences are based on comparison of each accession with the Col-0 reference genome. The accessions are aligned from top to bottom based on their phenotypic score for HopAM1-induced cell death (color code 5-4-3-2-1-0 = Red-Yellow-Green-Blue-White-Pink). Statistical significance for correlation between phenotypic scores and haplotype structure (absence of the three transposable elements: At2g15800, At2g15810 and At2g15815) was based on a type II ANOVA test (*p-value* = 0.002). High resolution image available as a supplemental file.

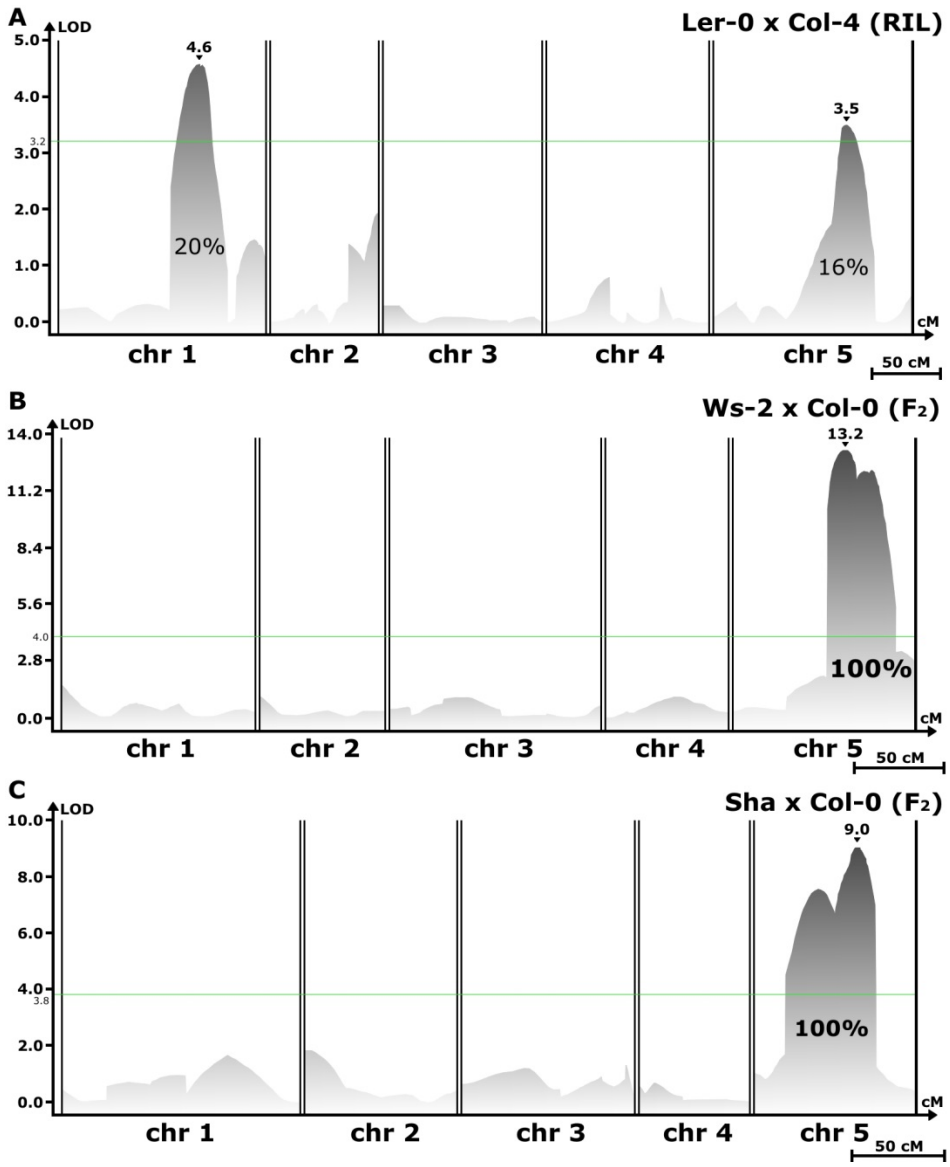

Figure S8 | Composite Interval Mapping on three different mapping populations. The analysis revealed two moderate effect loci on chromosomes 1 and 5 in Ler-0 x Col-4 background, and one locus on chromosome 5 in Ws-2 x Col-0 and Sha x Col-0background. The QTL in Ws-2 x Col-0 and Sha x Col-0 background appeared to be responsible for 100% of the phenotypic variance. The QTLs on chromosome 5 in each background is overlapping with QTL5A in the Bur-0 x Col-0 background. x-axis shows chromosomes 1 through 5 and map distances in cM. Peak LOD scores are shown by black triangles along with their values. Effects on phenotype variation are shown as percentages for each QTL. The global permutation level of significance was set at LOD 3.2 for Ler-0 x Col-4; LOD 4.0 for Ws-2 x Col-0; LOD 3.8 for Sha x Col-0.

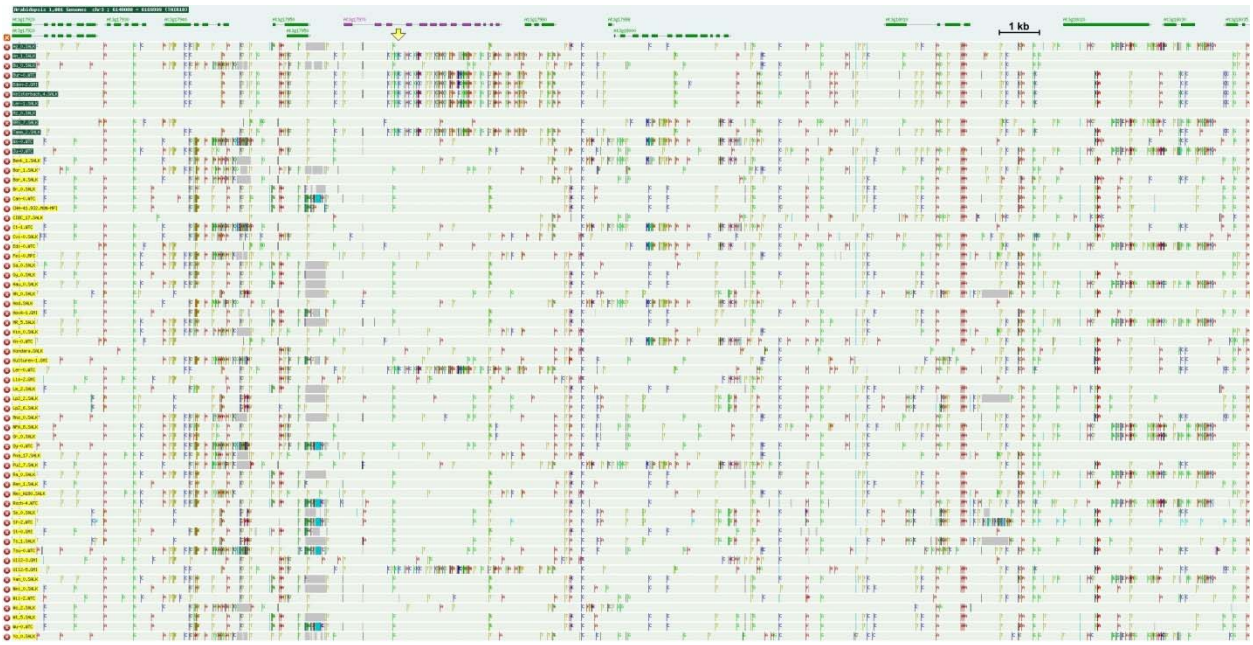

Figure S9 | Genomic alignment of accessions in relation to HopAM1-induced chlorosis near the most significant SNP. *A. thaliana* sequence differences are shown spanning a 30 kb region from 6140000 to 6170000, covering the area around the most significant SNP hit at 6150479 bp (shown by a yellow arrow). Sequence differences are based on comparison of each accession with the Col-0 reference genome. The accessions are aligned from top to bottom based on their phenotypic score for HopAM1-induced chlorosis (color code “0” = dark green/non-chlorotic, “1” = yellow/chlorotic). Statistical significance for correlation between phenotypic scores and haplotype structure (presence of multiple SNPs within At3g17970) was based on a type II ANOVA test (*p-value* = 0.015). High resolution image available as a supplemental file.

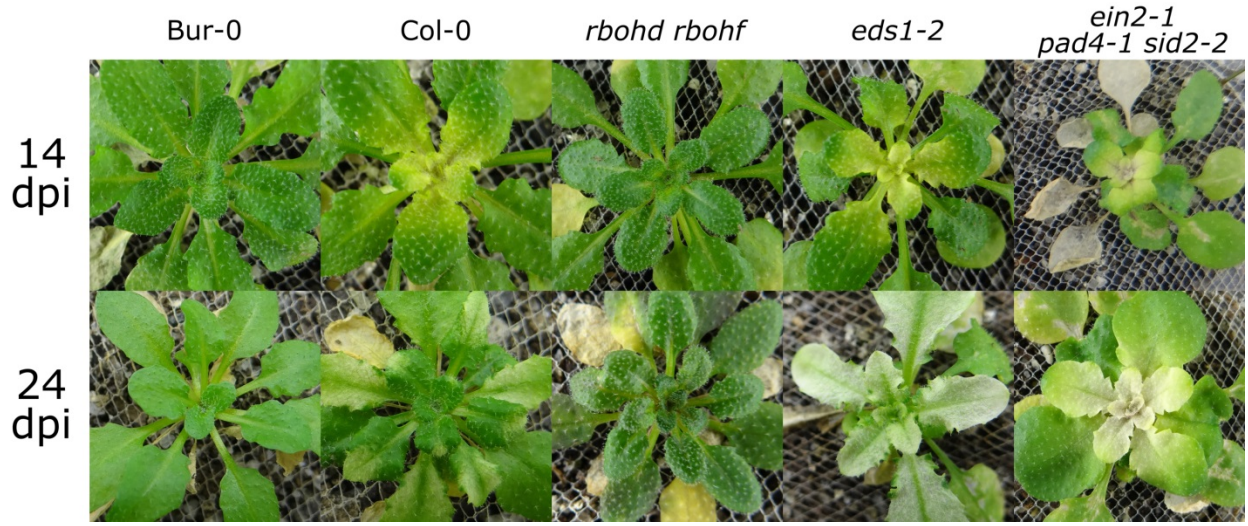

Figure S10 | HopAM1-induced rosette chlorosis is affected in *eds1-2* and *rbohd rbohf* backgrounds. Meristem chlorosis response following bacterial vacuum infiltration with *Pto* DC3000D28E(*hopAM1*). HopAM1-induced chlorosis in Bur-0, Col-0 and Col-0 *rbohd rbohf*, *eds1-2*, and *ein2-1 pad4-1 sid2-2* mutant lines at 14 dpi and 24dpi. The *rbohd rbohf* was the only mutant line that did not show chlorosis symptoms. Symptoms of prolonged chlorosis were observed at 24 dpi in the *eds1-2* and *ein2-1 pad4-1 sid2-2* plants, compared to the positive control Col-0 whose symptoms started to attenuate at 21 dpi. *Pto* DC3000D28E(*hopAM1*) OD_{600} = 0.05 (~$2.5x10^7$ cfu/ml). Statistical significance for correlation was based on simultaneous inference tests (Dunnett's t-tests). *rbohd rbohf* (*p-value* = 4.625e-06); *eds1-2* (*p-value* = 2.053e-06); *ein2-1 pad4-1 sid2-2* (*p-value* = 2.059e-06).

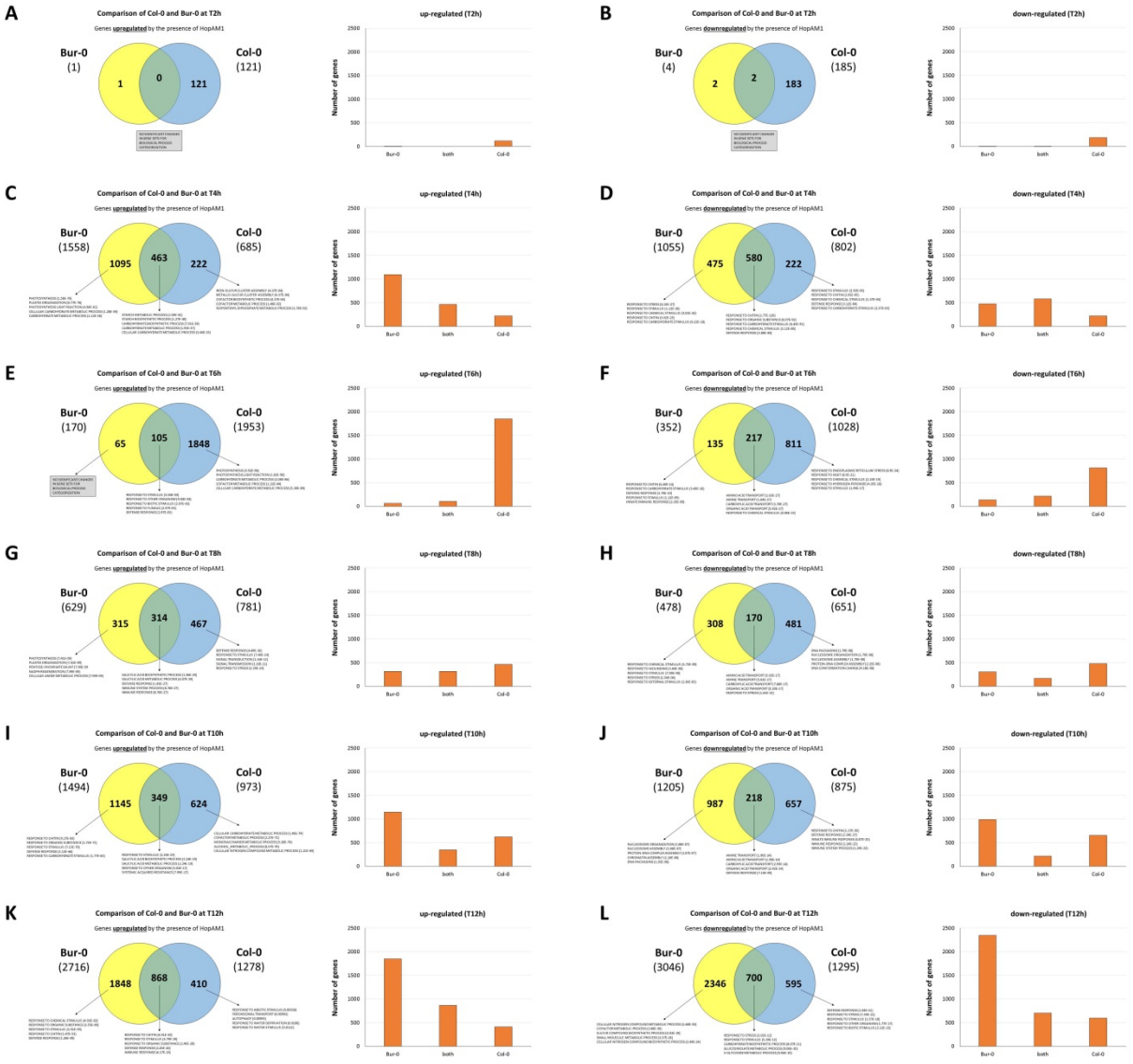

Figure S11 | Gene ontology enrichment analysis for differentially expressed genes in Bur-0 and Col-0 as a result of HopAM1 bacterial delivery. Number of genes is shown for each time point that is differentially regulated in each Venn diagram, along with the top five gene sets for each group. Time points show up-regulated (A, C, E, G, I, K) and downregulated (B, D, F, H, J, L) genes for 2 (A, B), 4 (C, D), 6 (E, F), 8 (G, H), 10 (I, J), and 12 hpi (K, L). *Pto* DC3000D28E(*hopAM1*) OD_{600} = 0.05 (~2.5x10^7 cfu/ml).

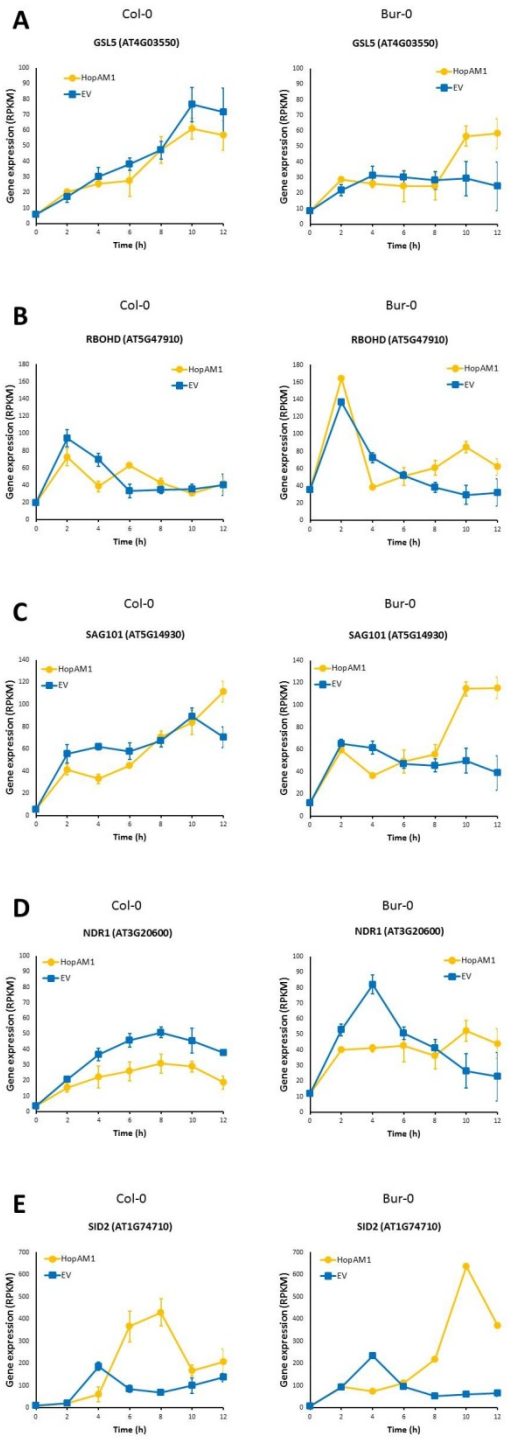

Figure S12 | HopAM1 changes the expression profile for key defense genes in Bur-0 at later timepoints. Expression profile of representative defense-related genes within the same time period in Col-0 and Bur-0.

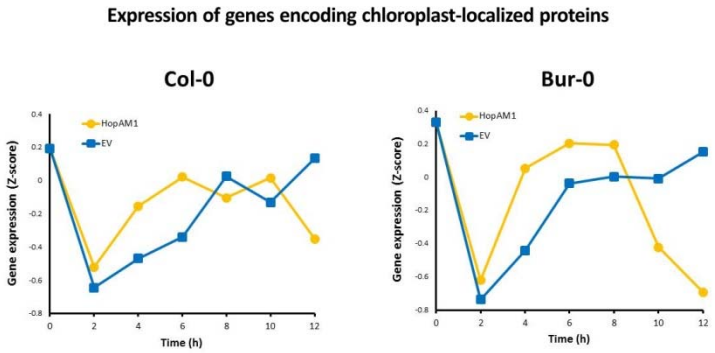

Figure S13 | HopAM1 down-regulates chloroplast-localized genes in Bur-0 and Col-0 at 12 hpi. Average transcriptional profile of over five thousand genes encoding chloroplast-localized proteins in both accessions. Results suggest that chloroplasts are one of the main targets of the transcriptional perturbations of HopAM1.

Table S1: List of bacterial strains and plasmid used in this study. (.xlsx, 11 KB)

Available for download as a .xlsx file at:

http://www.genetics.org/lookup/suppl/doi:10.1534/genetics.116.190678/-/DC1/TableS1.xlsx

Table S2: ANOVA tests and adjusted means of phenotypic scores for HopAM1-induced cell death response per RIL. (.xlsx, 18 KB)

Available for download as a .xlsx file at:

http://www.genetics.org/lookup/suppl/doi:10.1534/genetics.116.190678/-/DC1/TableS2.xlsx

Table S3: HopAM1-dependent cell death response is variable in Arabidopsis thaliana germplasm. (.xlsx, 11 KB)

Available for download as a .xlsx file at:

http://www.genetics.org/lookup/suppl/doi:10.1534/genetics.116.190678/-/DC1/TableS3.xlsx

Table S4: Bur-0 x Col-0 F_2 segregation ratios for HopAM1-induced cell death. (.xlsx, 11 KB)

Available for download as a .xlsx file at:

http://www.genetics.org/lookup/suppl/doi:10.1534/genetics.116.190678/-/DC1/TableS4.xlsx

Table S5: Reannotated Bur-0 x Col-0 RIL population. (.xlsx, 176 KB)

Available for download as a .xlsx file at:

http://www.genetics.org/lookup/suppl/doi:10.1534/genetics.116.190678/-/DC1/TableS5.xlsx

Table S6: Composite Interval Mapping result data for HopAM1-induced cell death on a Bur-0 x Col-0 RIL population. (.xlsx, 100 KB)

Available for download as a .xlsx file at:

http://www.genetics.org/lookup/suppl/doi:10.1534/genetics.116.190678/-/DC1/TableS6.xlsx

Table S7: Cell death QTL region gene edgeR results for the differential expression analysis (infected vs mock) in Bur-0 and Col-0 for all time points*. (.xlsx, 70 KB)

Available for download as a .xlsx file at:

http://www.genetics.org/lookup/suppl/doi:10.1534/genetics.116.190678/-/DC1/TableS7.xlsx

Table S8: ANOVA tables for pairwise interactions between QTLs for HopAM1-induced cell death. (.xlsx, 14 KB)

Available for download as a .xlsx file at:

http://www.genetics.org/lookup/suppl/doi:10.1534/genetics.116.190678/-/DC1/TableS8.xlsx

Table S9: List of top 10 SNP hits for HopAM1-induced cell death following Bonferroni correction. (.xlsx, 44 KB)

Available for download as a .xlsx file at:

http://www.genetics.org/lookup/suppl/doi:10.1534/genetics.116.190678/-/DC1/TableS9.xlsx

Table S10: Segregation ratios for HopAM1-induced cell death in three different mapping populations. (.xlsx, 84 KB)

Available for download as a .xlsx file at:

http://www.genetics.org/lookup/suppl/doi:10.1534/genetics.116.190678/-/DC1/TableS10.xlsx

Table S11: HopAM1-induced rosette chlorosis response in *Arabidopsis thaliana* germplasm. (.xlsx, 11 KB)

Available for download as a .xlsx file at:

http://www.genetics.org/lookup/suppl/doi:10.1534/genetics.116.190678/-/DC1/TableS11.xlsx

Table S12: ANOVA tests for HopAM1-induced chlorosis response per RIL. (.xlsx, 11 KB)

Available for download as a .xlsx file at:

http://www.genetics.org/lookup/suppl/doi:10.1534/genetics.116.190678/-/DC1/TableS12.xlsx

Table S13: Composite Interval Mapping result data for HopAM1-induced cell death on a Bur-0 x Col-0 RIL population. (.xlsx, 98 KB)

Available for download as a .xlsx file at:

http://www.genetics.org/lookup/suppl/doi:10.1534/genetics.116.190678/-/DC1/TableS13.xlsx

Table S14: List of top 10 SNP hits for meristem chlorosis following Bonferroni correction. (.xlsx, 47 KB)

Available for download as a .xlsx file at:

http://www.genetics.org/lookup/suppl/doi:10.1534/genetics.116.190678/-/DC1/TableS14.xlsx

Table S15: List of references for mutant Arabidopsis lines screened. (.xlsx, 19 KB)

Available for download as a .xlsx file at:

http://www.genetics.org/lookup/suppl/doi:10.1534/genetics.116.190678/-/DC1/TableS15.xlsx

Table S16: Complete edgeR results for the differential expression analysis (infected vs mock) in Bur-0 and Col-0 for all time points. (.xlsx, 7 MB)

Available for download as a .xlsx file at:

http://www.genetics.org/lookup/suppl/doi:10.1534/genetics.116.190678/-/DC1/TableS16.xlsx

Table S17: List of differentially regulated gene sets identified by ontology enrichment analysis at 4 hpi following inoculation with *Pto* DC3000D28E(*hopAM1*). (.xlsx, 86 KB)

Available for download as a .xlsx file at:

http://www.genetics.org/lookup/suppl/doi:10.1534/genetics.116.190678/-/DC1/TableS17.xlsx

Table S18: List of differentially regulated gene sets identified by ontology enrichment analysis at 6 hpi following inoculation with *Pto* DC3000D28E(*hopAM1*). (.xlsx, 70 KB)

Available for download as a .xlsx file at:

http://www.genetics.org/lookup/suppl/doi:10.1534/genetics.116.190678/-/DC1/TableS18.xlsx

Table S19: List of differentially regulated gene sets identified by ontology enrichment analysis at 8 hpi following inoculation with *Pto* DC3000D28E(*hopAM1*). (.xlsx, 62 KB)

Available for download as a .xlsx file at:

http://www.genetics.org/lookup/suppl/doi:10.1534/genetics.116.190678/-/DC1/TableS19.xlsx

Table S20: List of differentially regulated gene sets identified by ontology enrichment analysis at 10 hpi following inoculation with *Pto* DC3000D28E(*hopAM1*). (.xlsx, 80 KB)

Available for download as a .xlsx file at:

http://www.genetics.org/lookup/suppl/doi:10.1534/genetics.116.190678/-/DC1/TableS20.xlsx

Table S21: List of differentially regulated gene sets identified by ontology enrichment analysis at 12 hpi following inoculation with *Pto* DC3000D28E(*hopAM1*). (.xlsx, 79 KB)

Available for download as a .xlsx file at:

http://www.genetics.org/lookup/suppl/doi:10.1534/genetics.116.190678/-/DC1/TableS21.xlsx

Table S22: List of genes up-regulated and down-regulated by either *Pto* DC3000 effectors or HopAM1 alone in Col-0 at 12 hpi. (.xlsx, 5 MB)

Available for download as a .xlsx file at:

http://www.genetics.org/lookup/suppl/doi:10.1534/genetics.116.190678/-/DC1/TableS22.xlsx